Plant Communications
Research article

CellPress
Partner Journal

The Fie1-PRC2 complex regulates H3K27me3 deposition to balance endosperm filling and development in cereals

Jiechen Wang[1,10], Shuai Li[2,10], Liujie Wu[3,10], Dongsheng Shi[4], Lina Xu[1], Zhiping Zhang[1], Yongyan Wang[4], Chen Ji[1,5], Yuqi Chen[1,5], Xueling Zhou[3], Feifan Zhang[3], Mengyao Li[6], Xiaohan Li[6], Canghao Du[7], Qiong Wang[1], Xiaoduo Lu[8], Wenqin Wang[3], Guifeng Wang[4] and Yongrui Wu[1,9,*]

[1]State Key Laboratory of Plant Trait Design, CAS Center for Excellence in Molecular Plant Sciences, Shanghai Institute of Plant Physiology & Ecology, Shanghai 200032, China

[2]Shanghai Oebiotech Co., Ltd., Shanghai 200032, China

[3]College of Life Science, Shanghai Normal University, 100 Guilin Road, Shanghai 200233, China

[4]National Key Laboratory of Wheat and Maize Crops Science, College of Agronomy, Henan Agricultural University, Zhengzhou 450002, China

[5]University of the Chinese Academy of Sciences, Beijing 100049, China

[6]State Key Laboratory of Wheat Improvement, College of Life Sciences, Shandong Agricultural University, Tai'an 271018, China

[7]The Genetic Engineering International Cooperation Base of Chinese Ministry of Science and Technology, The Key Laboratory of Molecular Biophysics of Chinese Ministry of Education, College of Life Science and Technology, Huazhong University of Science & Technology, Wuhan 430074, China

[8]Institute of Molecular Breeding for Maize, Qilu Normal University, Jinan, China

[9]Shanghai Academy of Natural Sciences, Shanghai 200031, China

[10]These authors contributed equally to this article.

***Correspondence: Yongrui Wu (yrwu@cemps.ac.cn)**

https://doi.org/10.1016/j.xplc.2025.101343

ABSTRACT

Polycomb repressive complex 2 (PRC2)-mediated H3K27me3 deposition is vital for cell fate determination during *Arabidopsis thaliana* endosperm development. Unlike the transient endosperm in *Arabidopsis*, cereals follow a different developmental program after the cellularization phase, producing a persistent endosperm. In contrast to the single, constitutively expressed *Fertilization Independent Endosperm* (*FIE*) gene in *Arabidopsis*, cereals have evolved a duplicated, grain-specific counterpart, such as maize *ZmFie1* and rice *OsFie1*. However, their functions remain unclear. We applied Cleavage Under Targets and Tagmentation (CUT&Tag) to profile the dynamics of the H3K27me3 mark during maize endosperm development. We observed a genome-wide elevation of H3K27me3 levels at early stages, followed by a rapid reduction after seed filling. We identified common regions and designated them as Filling Specific Peaks (FSPs), which are largely regulated by *ZmFie1*. Indeed, knockout of *ZmFie1* results in earlier cellularization and slightly enhanced mitosis during endosperm filling, leading to smaller kernels that accumulate more zeins. Consistently, H3K27me3 levels on *α-zein* genes, located as tandem repeats on chromosome 4, are dramatically decreased in *zmfie1*. Moreover, it indirectly inhibits cell proliferation by mediating H3K27me3 deposition at *ZmMADS* loci, thereby balancing endosperm development and filling. Intriguingly, *OsFie1* imposes H3K27me3 modification at the loci of *13-kDa prolamin* genes and *OsMADSs*, leading to their repressed expression. Collectively, our findings reveal the conserved function of H3K27me3 deposition mediated by *ZmFie1*/*OsFie1* in cereal endosperm development. The newly evolved, cereal grain-specific FIE1-PRC2 complex plays a key role in balancing storage substance synthesis and cell proliferation during persistent endosperm development.

Key words: maize, ZmFie1, ZmPRC2, H3K27me3, endosperm filling, cell proliferation

Wang J., Li S., Wu L., Shi D., Xu L., Zhang Z., Wang Y., Ji C., Chen Y., Zhou X., Zhang F., Li M., Li X., Du C., Wang Q., Lu X., Wang W., Wang G., and Wu Y. (2025). The Fie1-PRC2 complex regulates H3K27me3 deposition to balance endosperm filling and development in cereals. Plant Comm. **6**, 101343.

INTRODUCTION

The endosperm is a storage organ in higher plants, characterized by a triploid chromosome ploidy. It serves as an energy reserve for embryo development and is a primary source of nutrition for both humans and animals. Endosperm development in dicotyledonous plants such as *Arabidopsis*, and in monocotyledonous plants such as maize, is fundamentally similar until the point of cellularization. After this stage, each species exhibits distinct patterns of cell fate determination (Sreenivasulu and Wobus, 2013). Following cellularization in *Arabidopsis*, the endosperm undergoes degradation, with nutrients being transferred to the cotyledons of the embryo. In contrast, the cellularized endosperm in cereals proceeds through cell proliferation, cell expansion, and tissue differentiation, ultimately developing into a functional organ for the synthesis and storage of substances. Endosperm filling in maize is coordinately regulated by transcription factors (TFs) such as *O2*, *PBF1*, and *NAC130*, which are highly expressed during this stage (Yang et al., 2023).

An open chromatin state is a prerequisite for the initiation of transcriptional activation. The Polycomb group (PcG) family catalyzes the trimethylation of lysine 27 on histone H3 (H3K27me3), an important transcriptional repressive modification that plays a crucial regulatory role at various developmental stages. The PRC2 complex primarily consists of SET domain methyltransferases, WD domain proteins, and ESC proteins. In *Arabidopsis*, the PRC2 complex restricts excessive cell proliferation during the early phase of endosperm development, thereby ensuring proper differentiation of endosperm cells (Grossniklaus et al., 1998; Ohad et al., 1999). All mutants of the *Arabidopsis* PRC2 complex exhibit endosperm over-proliferation following double fertilization, although the stage of developmental arrest varies slightly among them. The *msi1* mutant shows over-proliferation of the chalazal endosperm and fails to undergo cellularization (Kohler et al., 2003), whereas *fis* mutants display delayed cellularization of the peripheral endosperm (Sorensen et al., 2001). The *fie* mutants exhibit autonomous endosperm development in the absence of fertilization. After fertilization, *fie* mutants show abnormal development of both the endosperm and embryo, ultimately leading to infertility (Ohad et al., 1999).

The *Fie* gene in the grass family has undergone duplication and functional divergence. In wheat, seven copies of *TaFie* are located across three sets of chromosomes, but no grain-specific *TaFie* has been identified (Strejckova et al., 2020). In rice and maize, two members of the *Fie* gene have been identified in each species, namely *Fie1* and *Fie2*. *OsFie1* and *ZmFie1* show similar expression patterns, both specifically expressed during grain filling (Springer et al., 2002). However, *OsFie1* originated independently in the *Oryzeae* tribe, and *ZmFie1* and *ZmFie2* are more closely related to *OsFie2* (Cheng et al., 2020). The *osfie1* mutant has been reported to exhibit small grains and reduced storage protein content (Huang et al., 2016; Cheng et al., 2020; Wu et al., 2023). *ZmFie1* is a maternally imprinted gene in the endosperm, and its expression characteristics and imprinting regulation have been widely studied (Springer et al., 2002; Gutierrez-Marcos et al., 2006; Ni et al., 2019). However, its biological function during endosperm filling remains unknown.

The recent application of technologies such as Assay for Transposase-Accessible Chromatin using sequencing (ATAC-seq), Cleavage Under Targets and Tagmentation (CUT&Tag), and chromatin immunoprecipitation sequencing (ChIP-seq) has greatly advanced the study of epigenetic modifications during wheat endosperm development. Construction of an epigenetic regulatory network covering the development of the wheat embryo sac (0–4 days after pollination [DAP]) and endosperm (6–22 DAP) has revealed distinct regulatory mechanisms for starch and seed storage protein (SSP) synthesis in wheat (Zhao et al., 2024). The candidate TF *TaABI3A1* was found to promote SSP accumulation while simultaneously repressing starch synthesis and grain size increase. Meanwhile, another group of candidate TFs, TaNF-Y, interacts with the PRC2 complex and appears to inhibit gluten protein synthesis while promoting starch synthesis (Chen et al., 2024).

A novel wheat MADS gene, *TaMADS-GS*, has been identified as encoding a type I MADS-box TF. TaMADS-GS interacts with PRC2 to repress cytokinin oxidase/dehydrogenase (CKX)-encoding genes. Knockout of *TaMADS-GS* results in delayed endosperm cellularization and smaller kernel size (Zhang et al., 2024a). Data from wheat suggest that the primary function of H3K27me3 modification is to promote cellularization during early endosperm development and to inhibit gluten protein synthesis during the later filling stage.

Although the endosperm development process in grasses is similar, differences exist in the timing of key developmental stages. The duration of grain development and filling in maize is longer, and the final grain size is larger than that of rice and wheat. In wheat, endosperm cellularization is closely coupled with grain filling, with cellularization ending within a few days after pollination (typically 3–4 DAP), coinciding with the initiation of grain-filling gene expression (Xurun et al., 2015; Zhang et al., 2024a; Zhao et al., 2024). In contrast, although maize endosperm typically completes cellularization around 3–4 DAP, grain filling is initiated after 8 DAP. Between 4 and 8 DAP, the endosperm undergoes intense mitotic activity accompanied by a rapid increase in volume (Leroux et al., 2014; Ji et al., 2022). A recent study uncovered a unique regulatory network centered on the O2–ZmGRAS11–ZmEXPB15 module that coordinates grain filling and endosperm cell expansion (Ji et al., 2022). Unlike *ZmGRAS11*, which is specifically expressed in maize endosperm, its homologs in rice, *SLRL1* and *SLRL2*, are also highly expressed in leaves and stems (Itoh et al., 2005). Consistent with these distinct expression patterns, maize endosperm cells can enlarge up to 230 μm in length, resulting in a final grain length of up to 12 mm, whereas rice endosperm cells achieve a maximum length of only 100 μm, leading to a final grain length of just 6 mm (Song et al., 2007).

As the primary storage proteins in the maize endosperm, zeins are subdivided into four subclasses based on amino acid sequence homology: α (19 and 22 kDa), β (15 kDa), γ (50, 27, and 16 kDa), and δ (18 and 10 kDa) (Larkins et al., 2017). Transcripts from zein genes comprise approximately 65% of total transcripts during endosperm filling, with the 19-kDa *α-zein* and 22-kDa *α-zein* transcripts being the most prevalent, representing approximately 42% and 8% of transcripts, respectively (Chen et al., 2014).

In this study, we mapped the H3K27me3 histone modification landscape at five time points during maize endosperm development using CUT&Tag. Based on the data, we identified a group of H3K27me3 peaks specifically established at 8–10 DAP, termed Filling Specific Peaks (FSPs), the deposition of which is mediated by ZmFie1. Knockout of *ZmFie1* led to increased accumulation of zein proteins and a greater number of endosperm cells; however, it also resulted in reduced starch content and smaller grain size. ZmFie1 suppresses the premature expression of α-zeins by directly depositing H3K27me3 modifications at the tandem-repeat gene loci of *α-zeins* on chromosome 4. It also indirectly inhibits cell proliferation by mediating H3K27me3 deposition at the *ZmMADS* loci. These effects ultimately lead to balanced endosperm development and filling. Similarly, OsFie1 mediates H3K27me3 deposition at the loci of *13-kDa prolamin* genes and *OsMADSs*, leading to their repressed expression. Our findings reveal the conserved role of H3K27me3 deposition mediated by ZmFie1/OsFie1 in cereal endosperm development.

RESULTS

A group of ZmPRC2 members are highly expressed in maize endosperm before the onset of filling

The components of PRC2 in the maize genome and their interactions have been previously reported (Ni et al., 2019). By integrating published transcriptome data for maize endosperm, we identified the *PRC2* members expressed around the onset of endosperm filling. Expression data for the endosperm at 48–144 h after pollination (HAP) are derived from a study specifically focused on early maize endosperm development (Fu et al., 2023), whereas expression data for other developmental stages and tissues are sourced from a separate publication (Chen et al., 2014).

Near the onset of grain filling (from En6D to En10D, with D representing DAP), a group of PRC2 complex members are highly expressed, including *ZmFie1*, *ZmEmf2b*, *ZmMSI1c*, and *ZmMEZ1*. *ZmFie1*, in particular, is specifically expressed in the endosperm and begins to show high expression from En72HAP, a time point following completion of the coenocytic phase. In contrast, *ZmFie2* is ubiquitously expressed across all tissues and shows high expression during the coenocytic stage of endosperm development (En48HAP), with expression subsequently decreasing as development progresses (*ZmFie2 expression: En48HAP*, Fragments Per Kilobase of exon per Million mapped reads [FPKM] = 12.98; En10D, FPKM = 2.46). These data suggest that the PRC2 complex mediated by *ZmFie1* is the primary regulator during the En6D to En10D period. The other three members—*ZmEmf2b*, *ZmMSI1c*, and *ZmMEZ1*—although also expressed in other tissues, show their highest expression in the endosperm during 6–10 DAP (Supplemental Figure 1). The expression patterns of these genes suggest that H3K27me3 deposition mediated by the ZmFie1-PRC2 complex plays a significant regulatory role at the onset of endosperm grain filling.

Charting the H3K27me3 landscapes during maize endosperm filling

The PRC2 complex regulates plant development by repressing gene expression through the deposition of histone H3K27me3 modifications at specific genomic loci. We mapped the H3K27me3 landscapes of maize endosperm from 6 to 20 DAP using CUT&Tag with anti-H3K27me3 antibodies. Endosperm samples were collected from the B73 inbred line grown in Tai'an in spring 2023, and the developmental status at each time point was verified using free-hand sections. At 10 DAP, the endosperm appeared transparent, whereas the upper portion of the 12-DAP endosperm exhibited a pale-yellow coloration, indicating that visible storage substances had not yet accumulated at 10 DAP but had begun to accumulate by 12 DAP (Figure 1A).

Each time point included two replicates, yielding a total of 10 samples, and each sample was sequenced to a depth of 17 Gb (Supplemental Data 1). The correlation coefficient between the replicates at each time point exceeded 80%, indicating a high degree of consistency between biological replicates (Figure 1B). Unsupervised principal component analysis revealed a stage-specific transition pattern (Figure 1C).

Peak calling for each sample was performed using MACS2 software, resulting in the generation of a peak-calling dataset (Figure 1D, Supplemental Data 2). Although the number of H3K27me3 peaks was highest at 20 DAP, distribution of strong H3K27me3 signals along gene bodies was observed at 8 and 10 DAP, particularly with marked enrichment around the transcription start site (Figure 1E). By comparing peaks between adjacent time points, we identified stage-specific peaks (Supplemental Data 3). From 6 to 8 DAP, 8365 peaks were gained (Figure 1F), and from 10 to 12 DAP, 12 111 peaks were lost (Figure 1G)—a difference significantly greater than that observed between other periods (Figure 1H). Furthermore, the differential peaks gained and lost were more frequently observed in gene regions compared with those in other samples (Supplemental Figure 2). This suggests that these differential peaks have greater biological significance and are closely linked to changes in endosperm developmental status between 6 DAP and 12 DAP. Additionally, more peaks were lost between 10 and 12 DAP than were gained between 6 and 8 DAP, suggesting that some genes acquired peaks prior to or at 6 DAP, and all peak erasures occurred by 12 DAP. A total of 7084 new peaks were identified at 20 DAP, representing gene loci specifically silenced during the grain-filling period.

Distinct H3K27me3 modification features around endosperm filling

We found that a set of H3K27me3 modification peaks was gained prior to the onset of grain filling, whereas another set was lost after the grain-filling period officially began. Is there a correlation between the gain and loss of H3K27me3 peaks around the initiation of grain filling? To investigate this, we intersected the 8365 peaks gained from 8 DAP relative to 6 DAP with the 12 111 peaks lost from 12 DAP relative to 10 DAP, resulting in the identification of 5923 common peaks. These intersected peaks were designated as FSPs (Figure 2A). The 5923 FSPs corresponded to 2838 unique genes (Supplemental Data 4), which were significantly enriched for TF activity and nutrient reservoir activity (GO:0045735) (Figure 2B). Subsequently, we obtained a gene set of 1140 genes that specifically gained H3K27me3 marks between B8 and B6 (B8 gain-only), as well as a set of 3884 genes that specifically lost H3K27me3 marks between B12 and B10 (B12 loss-only). The top 30–50 expressed genes

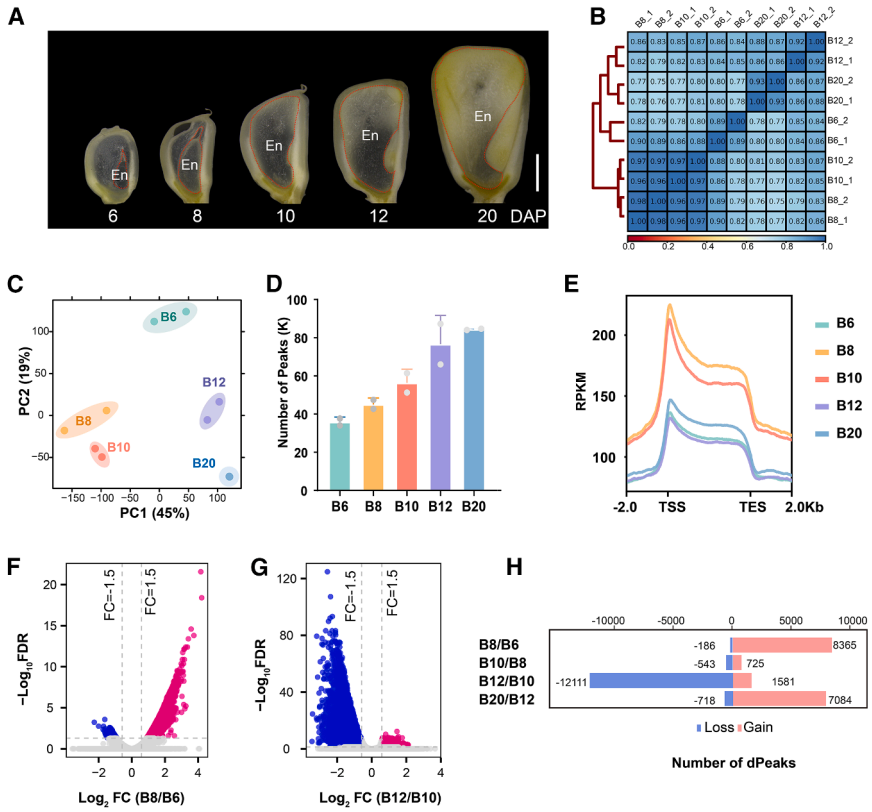

Figure 1. Charting the H3K27me3 landscapes during maize endosperm filling.

(A) Longitudinal free-hand sectioning of developing B73 kernels. Red dashed lines indicate the endosperm regions sampled for CUT&Tag. Bar, 2 mm.

(B) Heatmap showing Pearson correlation clustering of H3K27me3 modifications across developmental stages.

(C) Principal component analysis of H3K27me3 profiles.

(D) Number of H3K27me3 peaks in two biological replicates at each developmental time point.

(E) Metagene plots showing H3K27me3 distribution patterns across gene bodies at each developmental time point.

(F) Volcano plot showing log2 FC and statistical significance of differential H3K27me3 peaks between 6 and 8 DAP. FDR <0.05, FC absolute value >1.5.

(G) Volcano plot showing log2 FC and statistical significance of differential H3K27me3 peaks between 10 and 12 DAP. FDR <0.05, FC absolute value >1.5.

(H) Summary of distinct peak gains and losses between adjacent developmental stages.

in these three gene sets displayed distinctly different expression patterns during endosperm development. Among them, the FSP gene set showed a high, plateau-like expression pattern from En12 to En30; the B8/B6 gain-only gene set exhibited a high-front, low-back expression pattern from En6 to En38; and the B12/B10 loss-only gene set presented two expression types—some with a plateau-like pattern and others with a low-front, high-back pattern (Figure 2C).

We further analyzed the number of zein genes, starch synthesis genes (starch) and 34 key TFs (Ji et al., 2022) within these three gene sets (Supplemental Data 5). In the B73_v4 genome, there are 28 annotated zein genes, 16 of which belong to the FSP gene set, representing 57% of the total. Of the 34 starch synthesis genes, three (8%) are part of the FSP gene set, and 20 (59%) entirely lacked H3K27me3 modification. Among the 34 co-expressed TFs, eight (24%) were included in the FSP gene set, including *ZmNAC130* (Figure 2D). None of the zein genes, starch synthesis genes, or TF genes were included in the B8 gain-only gene set. The metagene plot of H3K27me3 distribution showed higher H3K27me3 signals along the gene bodies of zein genes and the 34 TFs at 8 and 10 DAP, whereas starch synthesis genes were largely devoid of H3K27me3 across all developmental stages (Figure 2E).

The distribution of H3K27me3 in the 1- to 19-Mb region of the short arm of Chr4 showed significant peaks in the tandem repeat regions of the *22-kD α-zein* and *19-kD z1A α-zein* loci, which increased from B6 to B8 and then decreased from B10 to B12. In regions outside the zein tandem repeats, differences in H3K27me3 peaks between time points were not significant (Figure 2F). Among the TFs co-expressed with grain-filling genes, *ZmNAC130*, *ZmNAC90*, *ZmNAC87*, *ZmNAC48*, *ZmTCP7*, *ZmMADS41*, *ZmIDD10*, *ZmMYB14*, *ZmARF23*, *ZmARF24*, *ZmTrihelix16*, and *ZmTALE74* demonstrated strong H3K27me3 signals at B8 and B10, whereas *O2* exhibited a distinct H3K27me3 modification pattern, peaking at B6 and gradually decreasing until B20. Furthermore, the PBF1 locus was largely devoid of H3K27me3 across all developmental stages (Supplemental Figure 3; Figure 2G).

These data reveal distinct H3K27me3 modification patterns between zein genes and starch synthesis genes. Although virtually no H3K27me3 signals were detected at starch synthesis gene loci, zein genes—particularly the tandemly repeated *22-kD α-zein* and *19-kD z1A α-zein* loci on Chr4—showed acquisition of H3K27me3 peaks before the initiation of grain filling (B6–B8), followed by their loss at B10–B12. Other zein gene loci located on different chromosomes, such as the *10-kD δ-zein*, *15-kD β-zein*, and *γ-zeins* (50, 27, and 16 kDa), exhibited little to no H3K27me3 enrichment (Supplemental Figure 3).

Enrichment analysis of the FSP genes revealed the presence of zein genes and a group of highly expressed TFs such as *ZmNAC130*. Based on expression patterns from En6 to En38, the FSP genes were classified into six clusters (Supplemental Figure 4), which displayed three distinct

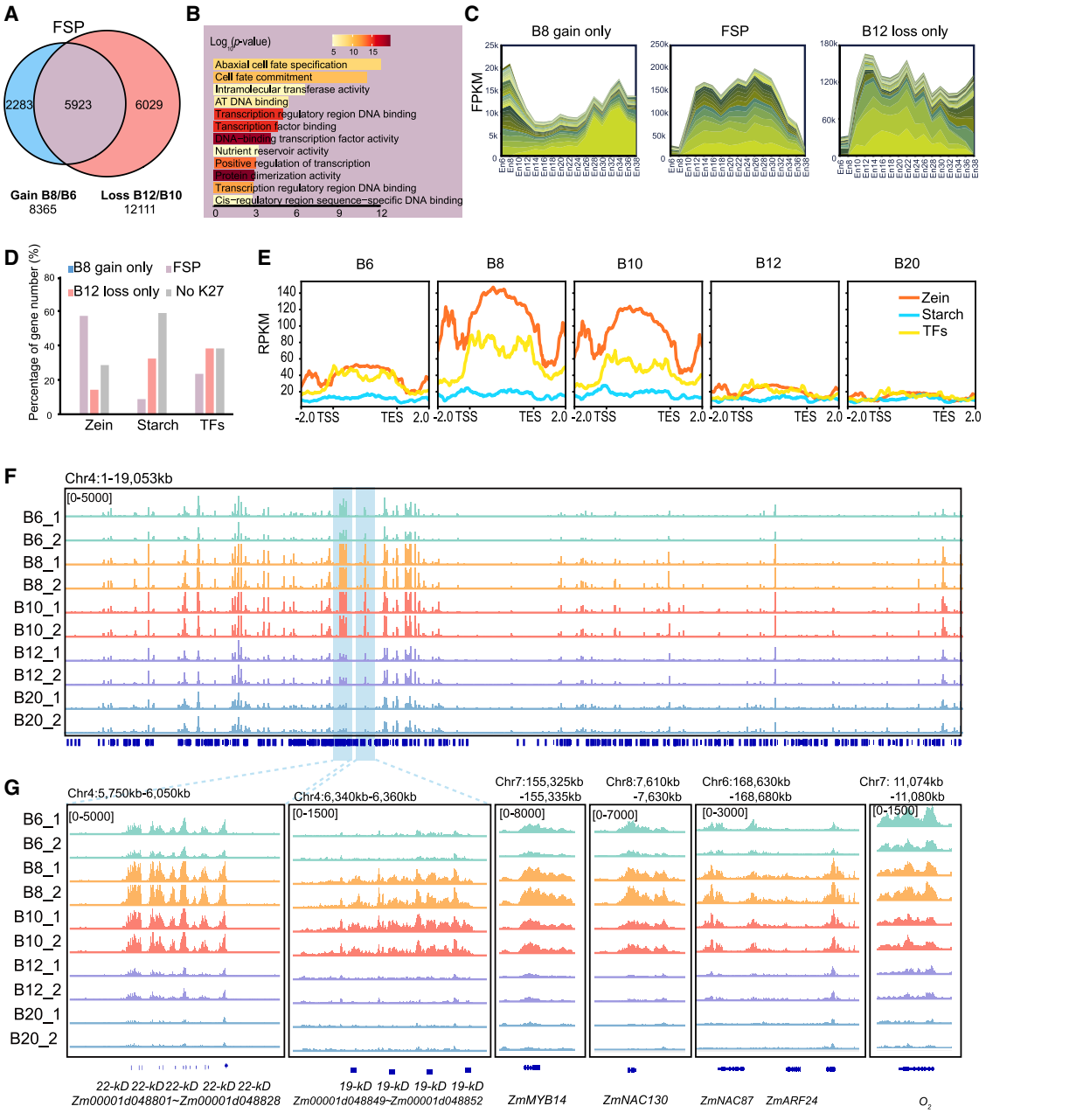

Figure 2. Distinct H3K27me3 modification features around the onset of endosperm filling.

(A) Venn diagram showing overlap between peaks gained from 6 to 8 DAP and peaks lost from 10 to 12 DAP.

(B) Gene ontology (GO) enrichment analysis of FSP genes.

(C) Stacked area chart showing expression patterns of three gene sets—B8 gain-only, FSP, and B12 loss-only—during endosperm development. Expression values were derived from public RNA-seq data (Chen et al., 2014).

(D) Proportions of starch synthesis genes, zein genes, and 34 TFs in each of the three gene sets.

(E) Metagene plot showing H3K27me3 density across loci of starch synthesis genes, zein genes, and 34 TFs from B6 to B20.

(F) IGV snapshots showing H3K27me3 distribution across the 1- to 19-Mb region of the short arm of chromosome 4. Blue regions indicate tandem repeat loci of the *22-kD* and *19-kD z1A zein* genes.

(G) Magnified views of the blue regions in **(F)**, along with other selected TF loci.

expression profiles: high then low (profiles 16 and 37), low then high (profile 43), and high in the middle (profiles 6, 44, and 11). The high-then-low type was the most common, comprising over 400 genes, most of which peaked at En6 and sharply declined after En8. This pattern is consistent with the typical role of H3K27me3 in gene repression. The low-then-high type showed increased expression after En20, aligning with reduced H3K27me3 modification after 12 DAP. The zein genes were predominantly assigned to profile 44, which exhibited a plateau-like expression pattern.

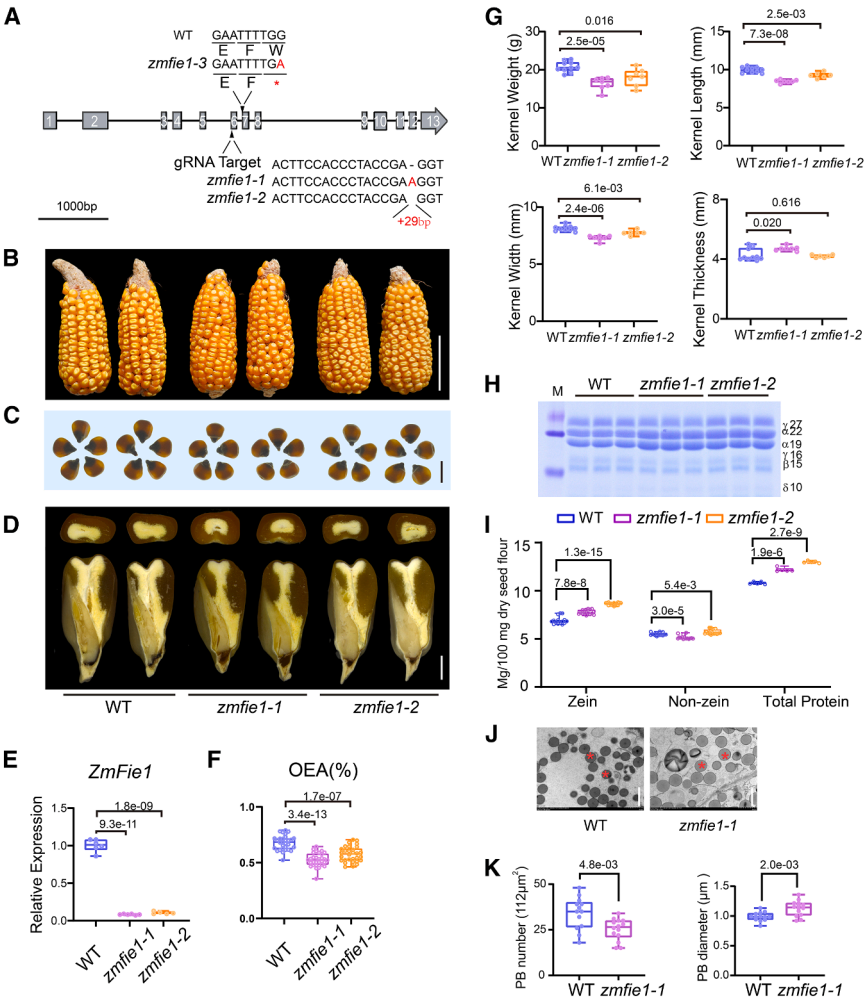

Figure 3. Reduced kernel size and increased α-zein in *zmfie1* mutants.

(A) Schematic representation of *zmfie1* alleles.

(B) Ear phenotypes of WT KN5585, *zmfie1-1*, and *zmfie1-2*. Scale bar, 5 cm.

(C) Kernel vitreousness of WT, *zmfie1-1*, and *zmfie1-2*. Scale bar, 1 cm.

(D) Transverse and longitudinal sections of WT, *zmfie1-1*, and *zmfie1-2*. Scale bar, 1 cm.

(E) RT-qPCR analysis of *ZmFie1* expression in 10-DAP endosperms of WT and *zmfie1* mutants. $n = 5$ biologically independent samples.

(F) Measurement of opaque endosperm area/total endosperm area in kernel transverse sections. Each value was derived from 30 kernels from three ears.

(G) Kernel weight (g), length (mm), width (mm), and thickness (mm) in WT and *zmfie1* mutants. $n = 6$–10 biologically independent ears.

(H) SDS–PAGE analysis of zeins in mature kernels of WT and *zmfie1* mutants. γ27, 27-kDa γ-zein; α22, 22-kDa α-zein; α19, 19-kDa α-zein; γ16, 16-kDa γ-zein; β15, 15-kDa β-zein; δ10, 10-kDa δ-zein.

(I) Zein, non-zein, and total protein content in the mature kernels of WT and *zmfie1*.

(J) TEM of WT and *zmfie1-1* endosperms at 24 DAP. Asterisk, protein body (PB).

(K) PB number and diameter in WT and *zmfie1-1* endosperms. PB, protein body. *p* values were determined by two-tailed Student's *t*-test.

zmfie1 loss-of-function mutants show reduced kernel size and increased α-zein content

To investigate the function of the ZmFie1-PRC2 complex in maize endosperm development, we generated two knockout lines using clustered regularly interspaced short palindromic repeats (CRISPR)/CRISPR-associated protein 9 (Cas9) in the maize inbred line KN5585 (designated *zmfie1-1* and *zmfie1-2*) and obtained one ethyl methanesulfonate (EMS)-induced mutant (named *zmfie1-3*; http://maizeems.qlnu.edu.cn/). The *zmfie1-1* mutant harbored an adenine insertion at position +746 base pairs (bp) relative to the start codon, whereas *zmfie1-2* had a 29-bp insertion at the same position (Figure 3A). Both mutations resulted in loss of *ZmFie1* function due to a frameshift causing premature termination. RT-PCR revealed that transcript levels of *ZmFie1* in 10-DAP *zmfie1-1* and *zmfie1-2* endosperms were dramatically reduced compared with those of the wild type (WT) (Figure 3E).

To examine kernel phenotypes in *zmfie1 mutants*, we planted *zmfie1-1*, *zmfie1-2*, and WT in Sanya (Figure 3B). Ears from the two mutant alleles that showed full seed set were used for photography and kernel trait measurements. On a light box, higher light transmission was observed in *zmfie1-1* and *zmfie1-2* kernels (Figure 3C). Longitudinal and transverse sections of the kernels revealed that the opaque endosperm ratio (opaque endosperm area [OEA] / total endosperm area) in *zmfie1-1* (52.5%) and *zmfie1-2* (57.5%) mutants was reduced compared to WT (67.8%) (Figures 3D and 3F; Supplemental Figure 6B). The 100-kernel weight was significantly lower than that of WT (Figure 3G). Kernel length and width were consistently reduced in *zmfie1* mutants; however, kernel thickness was slightly increased in *zmfie1-1* but remained unchanged in *zmfie1-2*.

To quantify storage substance content for each genotype, we selected five ears with uniform kernel size and full seed set. For each genotype, two kernels were sampled and ground into flour for analysis. SDS–PAGE analysis showed that the accumulation of 19- and 22-kDa α-zein proteins was notably increased in *zmfie1-1* and *zmfie1-2* mature kernels compared to WT, whereas the levels of other zeins remained unaffected (Figure 3H). Quantitative measurements revealed that total zein protein levels increased from 6.91% in WT to 7.77% in *zmfie1-1* and to 8.64% in *zmfie1-2*. Concurrently, non-zein protein levels slightly decreased in both *zmfie1-1* and *zmfie1-2* mutants. Given that the increase in zein content exceeded the reduction in non-zein content, total protein content was slightly enhanced in both mutants relative to WT (Figure 3I). Transmission electron microscopy of 24-DAP endosperms revealed that the diameter of protein bodies was significantly increased in *zmfie1-1*, with a slight

decrease in their number (Figures 3J and 3K), whereas the diameter of starch granules and total starch content were slightly reduced (Supplemental Figures 5A and 5B).

We also measured kernel traits of different genotypes segregated from the same ears, thereby eliminating the possibility that the observed differences between *zmfie1* mutants and WT resulted from environmental factors or ear-to-ear variation. Single kernels from self-pollinated *zmfie1-2*/+ heterozygous ears were phenotyped and then genotyped individually (Supplemental Figure 6A). The *ZmFie1*/*ZmFie1*, *ZmFie1*/*zmfie1-2*, and *zmfie1-2*/*zmfie1-2* genotypes segregated in a 1:2:1 ratio (Supplemental Figure 6C). The results showed that homozygous mutant kernels exhibited a significant reduction in single kernel weight and OEA, along with an increase in zein content. Starch content remained unchanged across genotypes (Supplemental Figure 6E).

The *zmfie1-3* allele in the B73 background was caused by a G/A substitution in the seventh exon of *ZmFie1*, resulting in a stop-gain mutation at tryptophan 271 (Figure 3A; Supplemental Figures 7A and 7B). We also found that the mRNA level of *ZmFie1* in the *zmfie1-3* endosperm at 8 DAP was decreased compared with that in the WT (Supplemental Figure 7C). Kernels from *zmfie1-3* plants, segregated from self-pollinated heterozygous ears, exhibited reduced OEA and increased zein content compared to those of WT B73 (Supplemental Figure 7D). However, no significant difference in kernel weight was observed between *zmfie1-3* and WT. The discrepancies in kernel weight phenotype between *zmfie1-1*/*zmfie1-2* and *zmfie1-3* might be attributed to differences in genetic backgrounds.

ZmFie1 mediates H3K27me3 deposition at filling-specific peaks (FSPs) and inhibits FSP gene expression

To investigate whether ZmFie1-PRC2 is responsible for H3K27me3 deposition at FSP loci, we performed H3K27me3 ChIP-seq on 10-DAP endosperms from WT and *zmfie1-1*. Additionally, we conducted RNA sequencing (RNA-seq) on the same samples (Supplemental Data 1 and 6).

We detected a total of 50 494 H3K27me3 peaks in WT-rep1 and 45 211 in WT-rep2. In contrast, *zmfie1*-rep1 and *zmfie1*-rep2 samples exhibited significantly more H3K27me3 peaks, with 66 367 and 94 743 peaks, respectively (Supplemental Data 5). The majority of H3K27me3 peaks in WT (68.67%) and *zmfie1* (62.80%) samples overlapped (Supplemental Figure 8A). Correlation analysis of peaks near genes revealed a strong correlation between the two WT replicates (r = 0.99), and between CUT&Tag and ChIP results (Supplemental Figure 8B, r = 0.64, Pearson's correlation).

The data reveal no significant differences in genome-wide H3K27me3 deposition between WT and *zmfie1*. Despite the higher number of H3K27me3 peaks, the overall H3K27me3 distribution along gene bodies appears to be slightly lower in *zmfie1* (Supplemental Figure 8C). A comparison of H3K27me3 profiles between WT and *zmfie1-1* identified 4339 lost peaks and 4953 gained peaks in *zmfie1-1* (Supplemental Data 6). Although the number of lost and gained H3K27me3 peaks in *zmfie1* did not show significant variation compared with WT, the lost peaks exhibited higher p values than the gained peaks (Figure 4A). Loci that gained H3K27me3 in *zmfie1* had almost no H3K27me3 deposition during endosperm development in WT. Conversely, loci that lost H3K27me3 in *zmfie1* exhibited high levels of H3K27me3 deposition during endosperm development in WT, particularly at 8 and 10 DAP (Supplemental Figure 8D).

We subsequently analyzed the overall impact of *zmfie1* deficiency on gene expression at 10 DAP using RNA-seq. Given the broad and subtle effects of H3K27me3 loss on gene expression, we used a q-value cutoff of ≤ 0.05 to identify differentially expressed genes, revealing 3904 upregulated genes and 3620 downregulated genes (Supplemental Figure 9A and Supplemental Data 7). Among the 4339 putative ZmFie1 targets, 335 genes were upregulated and 179 were downregulated in *zmfie1* compared to WT endosperm (Supplemental Figure 9B). The 335 ZmFie1-targeted genes that were upregulated exhibited a significant reduction in H3K27me3 signals in *zmfie1* endosperm. Surprisingly, the 179 ZmFie1-targeted genes that were downregulated also showed a significant decrease in H3K27me3 signals (Supplemental Figure 9C).

We further compared the previously identified FSPs with the *ZmFie1*-specific H3K27me3 peaks. A total of 1536 H3K27me3 peaks overlapped between the FSPs and *zmfie1* loss peaks, whereas only 45 H3K27me3 peaks overlapped between the FSPs and *zmfie1* gain peaks (Figure 4B and Supplemental Data 8). A general reduction of H3K27me3 was observed in *zmfie1* at the FSP loci, both in gene bodies and intergenic regions, which coincided with the upregulation of FSP gene expression (Figures 4C and 4D). When specifically examining the H3K27me3 profile of *zein* genes, TFs, and starch synthesis genes, we found no H3K27me3 signals at starch synthesis gene loci in either WT or *zmfie1*. In contrast, a significant reduction of H3K27me3 signals was observed for zein and TF loci in *zmfie1*. This reduction was most pronounced within the gene bodies of TFs and zein genes; it was also evident in the intergenic regions of *zein* genes (Figure 4E). The decrease in H3K27me3 signals at *zein* loci was accompanied by a general increase in *zein* gene expression, whereas the expression of starch synthesis genes remained unaffected in *zmfie1* endosperm. The situation for TFs was more complex: there was no overall change, but certain loci exhibited partial loss of H3K27me3 modification and, surprisingly, their expression was downregulated, as observed for *ZmMYB14* and *ZmNAC130* (Figure 4F and Supplemental Data 7).

Remarkably, the H3K27me3 profiles showed similar patterns at selected gene loci between the CUT&Tag and ChIP-seq datasets (Figure 4G). Furthermore, in the *zmfie1* mutant, the H3K27me3 profiles displayed a clear decreasing trend, particularly at the loci of α-*zein* genes on Chr4 and certain TFs. These findings support the hypothesis that the ZmFie1-PRC2 complex is partly responsible for H3K27me3 deposition at FSP sites and suppresses gene expression in these regions, especially at *zein* and TF loci.

We then performed GO enrichment analysis on the 335 upregulated *ZmFie1*-targeted genes, identifying six enriched GO terms, including histone methylation (GO:0016571) and nutrient reservoir activity (GO:0045735) (Supplemental Figure 9D). The nutrient reservoir activity category included 10 α-*zein* genes,

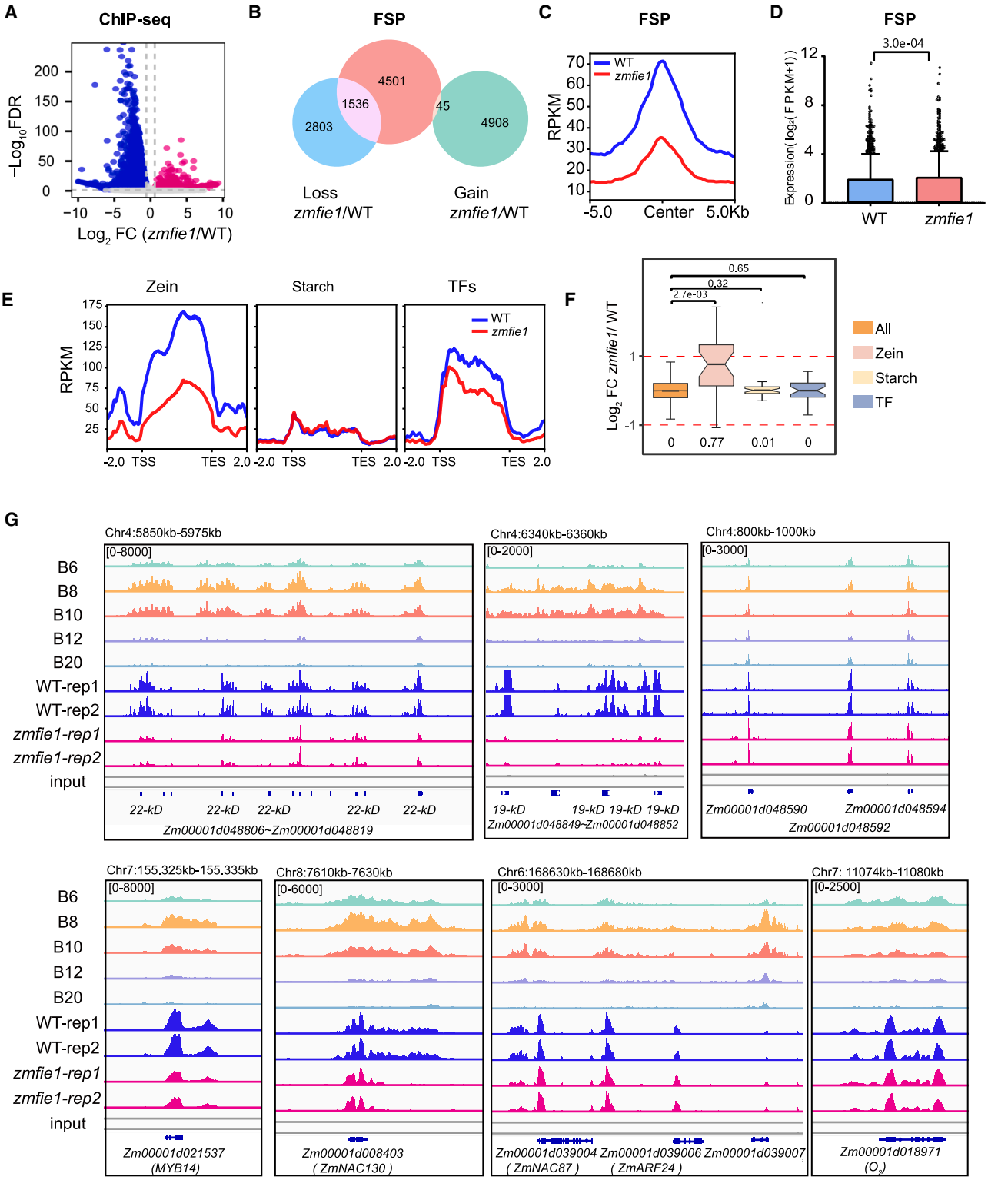

Figure 4. H3K27me3 patterns in WT and *zmfie1*.

(A) Volcano plot showing differences in H3K27me3 peaks between WT and *zmfie1-1*. Blue and red dots represent lost and gained peaks, respectively. FDR < 0.05, FC absolute value >1.5.

(B) Venn diagram showing overlap between FSPs and those lost or gained peaks in *zmfie1-1*.

(C) Metagene plot of H3K27me3 density at FSP loci in WT and *zmfie1-1*.

(legend continued on next page)

and the histone methylation category contained three methyltransferase genes: *Fie2* (*Zm00001d024698*), *MEZ1* (*Zm00001d036296*), and *SUVH5* (*Zm00001d032343*). The former two are members of the PRC2 complex responsible for H3K27me3 modification, whereas the latter is a homolog of *Arabidopsis thaliana SUVH5*, speculated to mediate H3K9me3 modification. H3K27me3 levels decreased at all three loci, coinciding with significantly increased gene expression in *zmfie1* (Supplemental Figures 9E and 9F). These findings suggest that the 4953 gained H3K27me3 peaks in *zmfie1* can be attributed to the upregulation of these methyltransferase genes. In contrast, loci where H3K27me3 signals decreased and gene expression increased in *zmfie1*, such as the α-*zein* loci, were not affected by methyltransferase upregulation.

ZmFie1 inhibits the transition from coenocyte to cellularization and the proliferation of endosperm cells

ZmFie1 is highly expressed from En3D to En10D. To elucidate the cause of the reduced grain size observed in *zmfie1* mutants, we collected kernel samples from *zmfie1-1* and WT from 2 to 10 DAP, covering the coenocytic stage through the initiation of grain filling. Cytological observations and analyses were conducted using nanoscale X-ray microscopy and semi-thin sections.

We monitored and quantified changes in endosperm size in *zmfie1* samples from 2 to 10 DAP. At 2 DAP, no significant differences in coenocyte morphology or size were observed between *zmfie1-1* and WT (Figure 5A; Supplemental Figure 10A). At 3 DAP, 10 sections were obtained from five ears each of WT and *zmfie1-1*. In nine of the 10 sections, *zmfie1-1* had already completed cellularization, with the central vacuole of the syncytium fully partitioned. In contrast, only two WT sections had completed cellularization; most WT endosperms had formed only 2–4 peripheral cell layers and were still undergoing the cellularization process. By 4 DAP, both WT and *zmfie1-1* had completed cellularization (Figure 5A). From 4 to 8 DAP, endosperm thickness in *zmfie1-1* was significantly less than that in the WT (Supplemental Figure 10). We counted the number of cells in the endosperm layer by layer from 4 to 10 DAP. At 4 DAP, the number of cells in *zmfie1-1* was lower than in the WT; however, from 8 to 10 DAP, *zmfie1-1 had a higher* number of endosperm cells than the WT (Figure 5B).

Kernel shape and cellular morphology during grain filling are significantly influenced by ear fertility and kernel arrangement. B73 kernels appear squarer and more flattened compared with those of KN5585. Consequently, we used *zmfie1-3* in the B73 background to investigate the impact of the *zmfie1* mutation on endosperm development. To elucidate the regulatory role of *ZmFie1* in endosperm cell development during the filling stage—and to eliminate variation due to developmental differences among ears—we selected WT and *zmfie1-3* kernels segregating from self-pollinated heterozygous ears at 16 DAP for cytological examination. The number of endosperm cells increased from 52.2 ± 2.55 in the WT to 60.50 ± 2.87 in *zmfie1-3*. However, endosperm thickness was reduced from 4.29 ± 0.28 mm in the WT to 3.89 ± 0.26 mm in *zmfie1-3*, and the average cell size was significantly reduced by 21.8% (Figures 5C and 5D). We then measured the cell width of each layer individually. Cell size was significantly reduced from the eighth to the 15th cell layer in the *zmfie1-3* endosperm (Figure 5E; Supplemental Data 9). In summary, *ZmFie1* appears to repress cell proliferation throughout endosperm development and inhibit the transition from coenocyte to cellularization.

Several MADS TFs are known PRC2 targets involved in regulating the timing of cellularization and endosperm cell proliferation, including *AGL62* (Kang et al., 2008) and *AGL37* (Masiero et al., 2011) in *Arabidopsis thaliana*, and *OsMADS77* and *OsMADS89* in rice (Tonosaki et al., 2021). A total of 98 *ZmMADS* genes have been identified in the maize genome (Zhao et al., 2021), and a list of cell-cycle-related genes in maize has been reported in a recent single-cell study (Yuan et al., 2024).

We analyzed H3K27me3 signals at the loci of *ZmMADS* genes and cell-cycle-related genes at various stages of endosperm development. H3K27me3 signals were nearly absent at the loci of cell-cycle-related genes throughout all stages. In contrast, strong H3K27me3 signals were detected at *ZmMADS* gene loci, peaking between 8 and 10 DAP, consistent with the peak distribution pattern of FSPs (Supplemental Figure 11A). In the *zmfie1-1* endosperm at 10 DAP, H3K27me3 levels at *ZmMADS* loci were significantly decreased, whereas the loci of cell-cycle-related genes maintained low signal levels without detectable differences between WT and *zmfie1-1* (Figure 5F). Overall expression of the G2/M phase cell cycle marker gene set was upregulated in zmfie1-1, whereas the S-phase marker gene set was downregulated. In contrast, the expression of MADS family genes varied; some genes were upregulated and others were downregulated (Figure 5G). Based on these findings, it is reasonable to speculate that certain MADS-type TFs might be direct downstream targets of the ZmFie1-PRC2 complex, whereas the cell-cycle-related genes are likely affected indirectly.

Next, we aimed to identify specific *ZmMADS* genes that may serve as direct downstream targets of ZmFie1-PRC2 and function in cell division regulation during early to mid-stages of endosperm development. Based on their expression patterns throughout endosperm development, we classified the 98 maize *MADS genes* into three groups: those specifically expressed at the 48-HAP coenocytic stage, those expressed between 72 HAP and 6 DAP, and those expressed at later stages (Supplemental Figure 11B). Of the 98 MADS genes, 33 overlapped with *zmfie1* peak loss regions, and 27 of these also belonged to the FSP gene set (Figure 5H). Among these 33 genes, nine were specifically expressed from 72 HAP to 6 DAP, 15 were specific to the 48-HAP coenocytic stage, and four were specifically expressed between 6 and 38 DAP. In the

(D) Boxplot showing expression levels of FSP genes in WT and *zmfie1-1*, based on RNA-seq data. *p* values were determined by Wilcoxon test. $^{***}p < 0.001$.
(E) Metagene plot showing H3K27me3 density at loci of starch synthesis genes, *zein* genes, and 34 TFs in WT and *zmfie1-1*.
(F) Boxplot showing log2 FC (*zmfie1-1*/WT) for each gene set. *p* values were determined by Wilcoxon test.
(G) IGV snapshots showing H3K27me3 distribution at loci of the *22-kD* and *19-kD z1A zein* genes, as well as selected TFs.

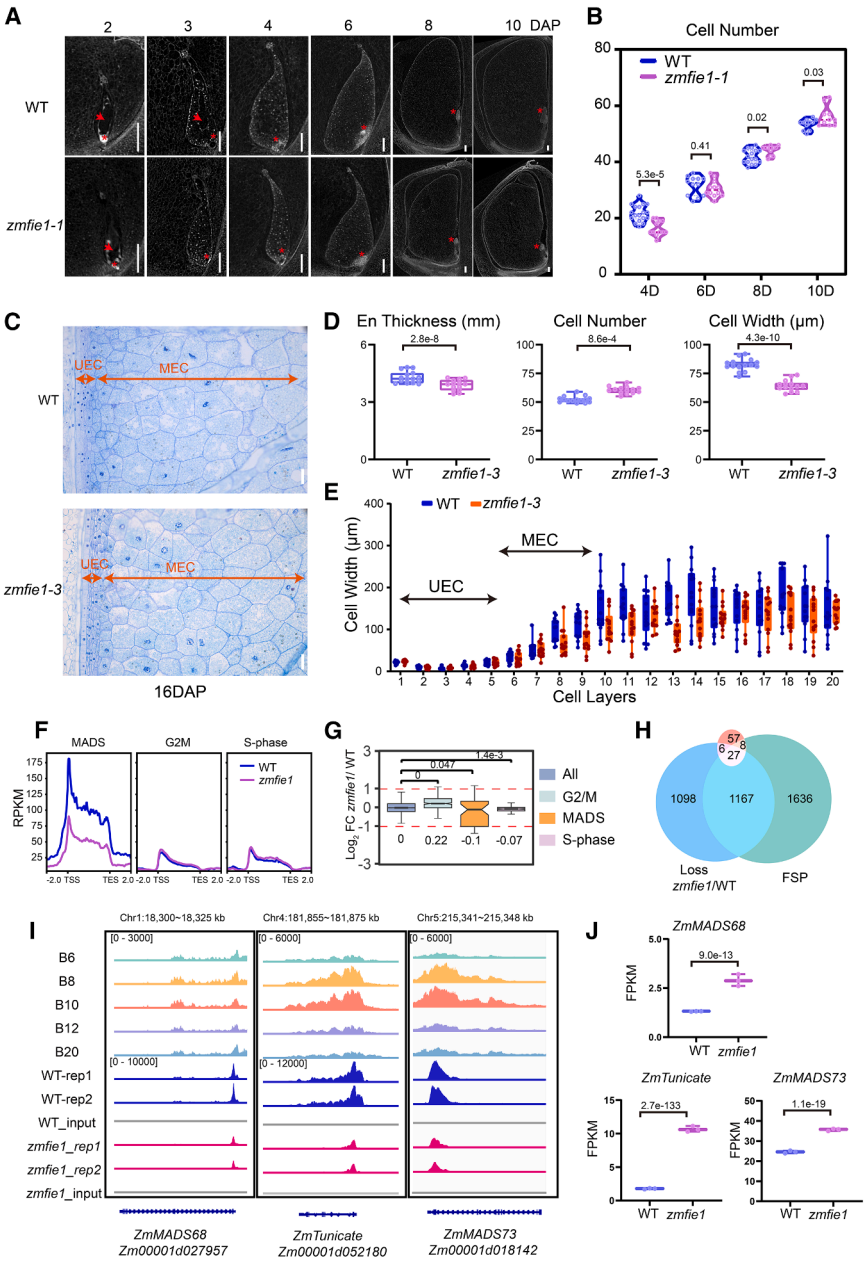

Figure 5. Premature cellularization and enhanced cell proliferation in the *zmfie1* endosperm.

(A) Longitudinal sections of developing WT and *zmfie1-1* endosperms visualized by X-ray computed tomography (CT). Scale bars, 200 μm. Asterisk, embryo; arrow, central vacuole.

(B) Violin plot showing cell counts in WT and *zmfie1-1* endosperms from 4 to 10 DAP.

(C) Light microscopy images of semi-thin sections of WT and *zmfie1-3* endosperms at 16 DAP. Scale bar, 50 μm.

(D) Measurements of endosperm thickness (mm), cell number, and cell width (μm) in WT and *zmfie1-3*. Data are presented as mean values ±SD, n = 15 biologically independent samples for endosperm thickness, cell width, and cell number. p values were determined by two-tailed Student's t-test.

(E) Cell width (μm) measured layer by layer across 16-DAP endosperms in WT and *zmfie1-3*. Data are presented as mean values ±SD, n = 14 biologically independent samples.

(F) Metagene plot showing H3K27me3 density at loci of *MADS* genes and cell-cycle marker genes in WT and *zmfie1-1*.

(G) Boxplot showing log2 FC (*zmfie1-1*/WT) for each gene set. p values were determined by Wilcoxon test. $^{***}p < 0.001$, $^{**}p < 0.01$, $^{*}p < 0.05$.

(H) Venn diagram showing overlapping genes between FSP genes and loss-peak genes in *zmfie1-1*.

(I) IGV snapshots showing H3K27me3 distribution at *MADS* gene loci in WT and *zmfie1-1*.

(J) Transcript levels of *MADS* genes in WT and *zmfie1-1*, based on RNA-seq data.

zmfie1-1 endosperm at 10 DAP, despite the overall decrease in H3K27me3 levels at these loci, only three genes (*Zm00001d018142*, *Zm00001d052180*, and *Zm00001d027957*) were significantly upregulated (Figures 5I and 5J). In the *zmfie1-1* mutant, the upregulation of these three *MADS* genes may contribute to the slight increase in cell number observed in the 10-DAP *zmfie1-1* endosperm.

On the other hand, imprinted genes are predominantly associated with the regulation of cellularization, with PRC2 acting as a key regulator by inhibiting the maternal expression of paternally expressed genes (PEGs). Based on the list of maternally expressed genes (MEGs) and PEGs from the literature (Anderson et al., 2021), PEG loci were found to exhibit high H3K27me3 signals, which dramatically decreased in the *zmfie1-1* endosperm at 10 DAP, accompanied by significant upregulation of PEG gene expression. In contrast, MEG loci maintained low H3K27me3 signal levels, showing no significant changes between WT and *zmfie1-1*, and exhibited decreased gene expression (Supplemental Figures 12A and 12B). Specifically, among the conserved PEGs, *ARID1* (*Zm00001d032832*) and *ARID9* (*Zm00001d032096*) exhibited reduced H3K27me3 modification without changes in gene expression in *zmfie1-1*, whereas *VIM104* (*Zm00001d019342*) showed reduced H3K27me3 levels and increased gene expression. Among the MEG genes, *O1* (*Zm00001d052110*) and *NRP1* (*Zm00001d040189*) displayed decreased H3K27me3 modification and increased expression in *zmfie1-1*, whereas *Fl3* (*Zm00001d009292*) exhibited a different H3K27me3 modification pattern (Supplemental Figures 12C and 12D).

These findings suggest that the ZmFie1-PRC2 complex inhibits premature cellularization and represses cell proliferation throughout endosperm development. This function may be mediated through extensive H3K27me3 modifications at *MADS* gene

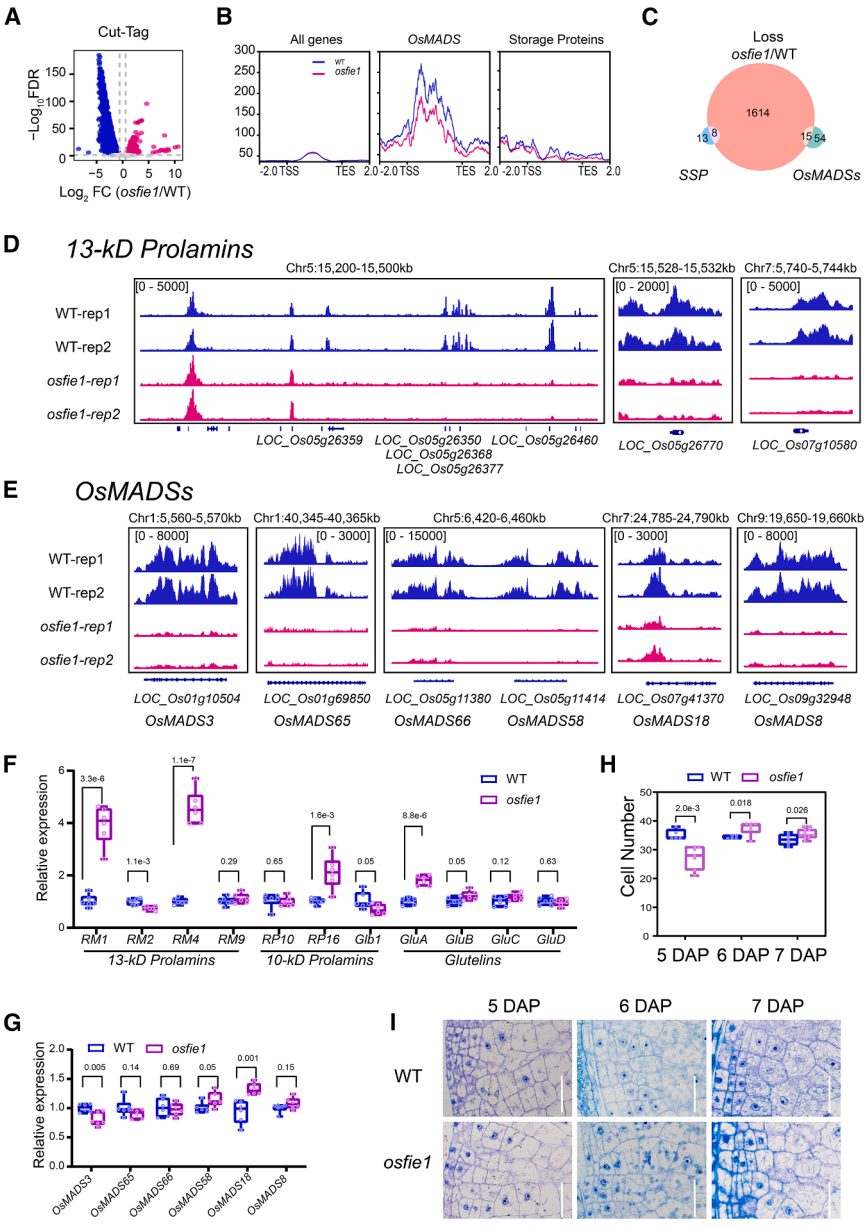

Figure 6. Enhanced cell proliferation and increased expression of *13-kDa prolamin* genes in *osfie1* due to reduced H3K27me3 deposition.

(A) Volcano plot showing variation in H3K27me3 peaks between WT and os*fie1*. Blue and red dots represent lost and gained peaks, respectively. FDR < 0.05, FC absolute value >1.5.

(B) Metagene plot showing H3K27me3 density across the genome at the loci of *MADS* genes and storage-protein genes in WT and os*fie1*.

(C) Venn diagram showing overlap among *MADS* genes, storage-protein genes, and loss-peak-genes in *osfie1*.

(D) IGV snapshots showing H3K27me3 distribution at *13-kDa prolamin* loci in WT and *osfie1*.

(E) IGV snapshots showing H3K27me3 distribution at *OsMADS* loci in WT and *osfie1*.

(F) RT-qPCR analysis of storage-protein gene expression in 5-DAP WT and *osfie1* endosperms. $n = 5$ biologically independent samples.

(G) RT-qPCR analysis of *OsMADS* gene expression in 5-DAP WT and *osfie1* endosperms. $n = 5$ biologically independent samples.

(H) Cell number in WT and *osfie1* endosperms at 5, 6, and 7 DAP. Data are presented as mean values ±SD, n = 5–10 biologically independent samples. p values were determined by two-tailed Student's t-test.

(I) Light microscopy images of semi-thin sections of WT and os*fie1-3* endosperms at 5, 6, and 7 DAP. Scale bar, 50 μm.

loci, suppressing the expression of distinct *MADS* genes at different developmental stages.

OsFie1-mediated H3K27me3 deposition at *13-kDa prolamin* and *OsMADS* loci inhibits their expression

The expression patterns of *ZmFie1* in maize and *OsFie1* in rice are similar. Although many studies have reported the phenotypes of *osfie1* mutants, it remains unclear whether *OsFie1* regulates the synthesis of storage proteins and cell proliferation in the rice endosperm (Huang et al., 2016; Cheng et al., 2020; Wu et al., 2023).

We selected a null allele of *osfie1* to study the function of *OsFie1* (Cheng et al., 2020). We collected 5-DAP caryopses for H3K27me3 CUT&Tag analysis and performed RT-qPCR on the same set of samples. Comparison of H3K27me3 profiles between WT and *osfie1* revealed 2596 lost peaks and 1960 gained peaks (false discovery rate [FDR] <0.05, absolute fold change [FC] >1.5) (Figure 6A; Supplemental Data 10). The higher number of lost peaks with high p values suggests a direct effect of loss of *Osfie1* function. No significant differences in H3K27me3 deposition were observed between WT and *osfie1*, including at storage-protein loci. However, a general reduction of H3K27me3 was observed in *osfie1* at *OsMADS* loci within gene-body regions (Figure 6B).

A total of eight rice storage-protein genes were identified among the *osfie1* lost-peak gene set (He et al., 2021). Seven of these genes were located in the *13-kDa prolamin* tandem-repeat region on chromosome 5 (RM4 cluster), and the remaining gene, *LOC_Os07g10580*, was located on chromosome 7 (RM1 cluster) (Figures 6C and 6D). Consistent with the decrease in H3K27me3 modification, both the *RM4 prolamin* cluster on chromosome 5 and the *RM1 prolamin* gene *LOC_Os07g10580* showed a four-fold significant increase in expression (Figure 6F). However, no obvious difference was observed in the total storage protein content or 13-kDa prolamin levels between mature grains of WT and the *osfie1* mutant (Supplemental Figure 13).

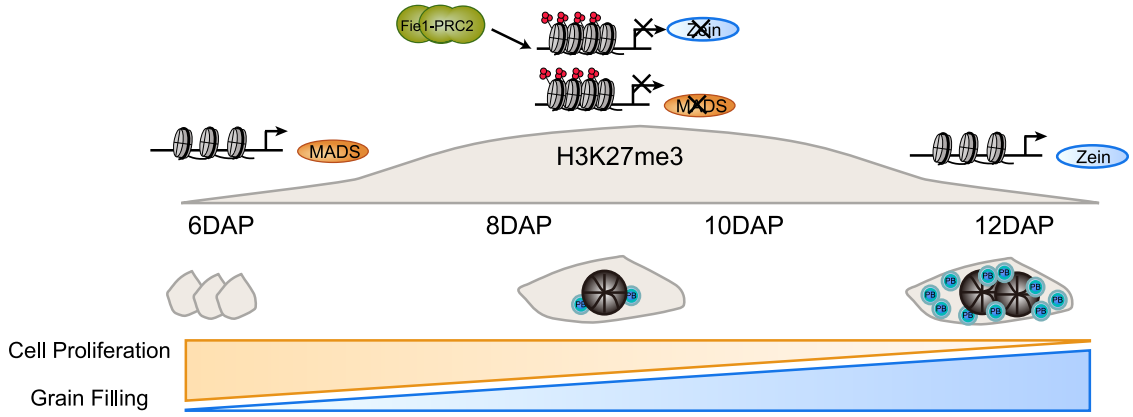

Figure 7. A proposed model for Fie1-PRC2.
Fie1-PRC2 mediates H3K27me3 deposition at the *zein* and *MADS* loci to inhibit their expression, balancing endosperm development and filling. Six DAP represents the early stage of endosperm development, when cells are small. The 8–10 DAP window marks the onset of endosperm filling, during which starch and storage proteins begin to accumulate, accompanied by notable cell expansion. After 12 DAP, the endosperm enters an active filling phase characterized by substantial storage compound synthesis. MADS-box TFs likely regulate endosperm cell proliferation, whereas zein genes encode major storage proteins that assemble into specialized protein bodies within the endosperm.

Sixty-nine *OsMADS* genes have been identified in the rice genome (Cheng et al., 2020), of which 15 were found in the *osfie1* lost-peak gene set (Figure 6C). Among these, *OsMADS1*, *OsMADS3*, *OsMADS5*, *OsMADS8*, *OsMADS64*, *OsMADS65*, and *OsMADS77* have been reported to participate in early endosperm cell proliferation (Tonosaki et al., 2021). In our data, a general decrease in H3K27me3 modification was observed at the *OsMADS3*, *OsMADS8*, *OsMADS18*, *OsMADS58*, *OsMADS65*, and *OsMADS66* loci in *osfie1*; however, only *OsMADS8*, *OsMADS18*, and *OsMADS58* showed upregulated expression (Figures 6E and 6G).

We also collected caryopses at 5, 6, and 7 DAP for semi-thin sections. The number of cells along the widest axis of the caryopsis remained unchanged from 5 to 7 DAP in the WT, averaging approximately 34 layers. Although the *osfie1* mutant had fewer cells than the WT at 5 DAP, the number of cells increased from 27.3 ± 3.6 at 5 DAP to 37.5 ± 2.4 at 6 DAP, which was significantly higher than that observed in the WT at 6 DAP (Figures 6H and 6I). At 7 DAP, the cell number remained stable in the *osfie1* mutant.

Taken together, these data indicate that the functions of *OsFie1* in rice and *ZmFie1* in maize are conserved with respect to the regulation of cell proliferation and expression of storage-protein genes.

DISCUSSION

The *ZmFie1* gene, which encodes a component of the PRC2 complex, exhibits a specific expression pattern during endosperm development. Although *ZmFie1* was identified 20 years ago (Danilevskaya et al., 2003), the full extent of its biological roles has not been thoroughly investigated. In this study, we comprehensively mapped the H3K27me3 modification landscape during maize endosperm development, with particular focus on the period surrounding the initiation of filling. This analysis led to the identification of a set of H3K27me3 modification peaks associated with the initiation of filling, termed FSPs. The specific deposition of H3K27me3 at FSPs—partly mediated by ZmFie1—is crucial for the coordinated regulation of cell proliferation and zein protein synthesis during the onset of endosperm filling (Figure 7).

The Fie1-PRC2 complex balances endosperm development and storage substance synthesis during endosperm filling

Based on their expression patterns during maize endosperm development, FSP genes can be categorized into two types. The first type, represented by *ZmMADS* genes, exhibits high expression before 6 DAP. From 6 to 8 DAP, an increase in H3K27me3 modification at *ZmMADS* loci is accompanied by a reduction in gene expression, consistent with the classical repressive role of H3K27me3. From 10 to 12 DAP, the loss of FSPs at *ZmMADS* loci does not lead to gene reactivation. Similarly, in *zmfie1* and *osfie1* mutants, a significant reduction in H3K27me3 at MADS loci results in only minor gene upregulation. This may be due to the conversion of reversible H3K27me3 marks into more stable DNA methylation at these loci, suggesting that the reduction of H3K27me3 is necessary but not sufficient for gene activation.

The second type is represented by zein genes. From 6 to 8 DAP, zein gene expression increases alongside a significant rise in H3K27me3 modification at their loci. From 10 to 12 DAP, the reduction in H3K27me3 is accompanied by a sharp increase in gene expression. In animal embryonic development, bivalent promoters—marked by both the activating modification H3K4me3 and the repressive H3K27me3—are thought to maintain developmental genes in a primed state, ready for rapid activation during differentiation (Macrae et al., 2023; Zhu et al., 2023). Zein gene loci from 6 to 8 DAP may resemble a similar bivalent promoter state. Between 10 and 12 DAP, the loss of H3K27me3 is likely accompanied by the acquisition of activating epigenetic marks, further enhancing zein gene expression.

H3K27me3 modification mediated by the Fie1-PRC2 complex at the onset of grain filling represses premature expression of zein genes and prevents excessive proliferation of endosperm cells, thereby promoting balanced endosperm development and storage substance synthesis.

The PRC2 complex inhibits endosperm cell proliferation from 3 to 16 DAP

Research on the function of PRC2 in endosperm cell proliferation has primarily focused on the critical transition from the coenocytic phase to cellularization. In *Arabidopsis*, most *prc2* mutants exhibit excessive proliferation of coenocytic nuclei and delayed or incomplete cellularization (Olsen, 2001; Sorensen et al., 2001). Downstream of *PRC2*, *mads* mutants such as *agl62* and *agl*80 display reduced numbers of coenocytic nuclei and earlier onset of cellularization (Portereiko et al., 2006; Kang et al., 2008; Wang et al., 2020b). However, exceptions have been reported—for instance, the *bbm* mutant shows reduced coenocytic nuclei and delayed cellularization (Chen et al., 2022), whereas *agl9* and *agl15* mutants display delayed cellularization without noticeable changes in the number of endosperm nuclei (Zhang et al., 2024b). These findings indicate that coenocytic nuclear proliferation and the timing of cellularization in *Arabidopsis* are not fully coupled, and that the final size of the endosperm is determined by the coordinated outcome of both processes.

Unlike the transient endosperm in *Arabidopsis*, which is degraded early in development, the endosperm in maize and other species of the Poaceae family undergoes prolonged mitosis and differentiation, coupled with storage substance synthesis. *ZmFie2* and *ZmFie1* exhibit complementary expression patterns during endosperm development (Supplemental Figure 1). The premature cellularization phenotype in *zmfie1* may result from specific regulation of cellularization by the *Fie1*-PRC2 complex or from compensatory upregulation of *ZmFie2*. At 4 DAP in *zmfie1* and 5 DAP in *osfie1,* cell numbers are reduced compared to WT, consistent with premature cellularization. In contrast, the increase in cell numbers from 8 to 10 DAP in *zmfie1* and from 6 to 7 DAP in *osfie1* likely reflects elevated rates of cell proliferation relative to WT. Additionally, in the *zmfie1* mutant, reduction of H3K27me3 modification at PEG loci is accompanied by increased gene expression, whereas MEG loci show minimal H3K27me3 signals. This implies that PEGs likely function downstream of PRC2 and contribute to the regulation of cellularization in maize.

Our data confirm that the ZmFie1-PRC2 complex represses endosperm cell proliferation from 3 to 16 DAP (Figures 5A–5E). At 3 DAP, the onset of premature cellularization is inhibited; between 4 and 10 DAP, excessive cell proliferation is suppressed; and by 16 DAP, proliferation is further restrained alongside the promotion of cell expansion. We hypothesize that the ZmFie2-PRC2 complex is active during the coenocytic stage, whereas ZmFie1-PRC2 functions from the cellularization stage through the grain-filling stage.

However, we also observed upregulation of *ZmFie2* expression and the emergence of novel H3K27me3 peaks in the *zmfie1* mutant. This suggests that functional characterization of the ZmFie1-PRC2 complex during endosperm development may be confounded by compensatory effects mediated by *ZmFie2*.

The Fie1-PRC2-prolamin module is conserved among cereals

Prolamins are seed storage proteins in cereals that differ in proportion and function across species. The prolamin gene family is highly complex due to dispersed and tandem amplification. In maize, prolamins are known as zeins. Approximately 60% of total kernel protein is zein, of which around 60% are α-zeins. Genes encoding α-zeins are primarily arranged in tandem repeats on chromosome 4 and exhibit substantial variation among maize inbred lines (Dong et al., 2016). In rice, prolamins are not the predominant storage proteins; they are classified into three categories based on molecular weight, with the 13-kDa prolamins arranged in tandem on chromosome 5 (Xu and Messing, 2008). In Triticeae, the major storage proteins are S-rich prolamins, including α/β-gliadin, γ-gliadin, and low-molecular-weight glutenin (Wang et al. 2020a).

The core functions of PRC2 are conserved in cereals. However, genome duplication and the unique biological features of grasses have led to an expansion in the number of PRC2 members and functional diversification. Through detailed analysis of *TaFie* expression patterns across multiple transcriptome datasets, we identified specific high expression of *TaFIE-7A2.2*, *TaFIE-4A1*, and *TaFIE-7D1* during early endosperm development, suggesting the presence of grain-specific *FIE* members in wheat as well (Supplemental Data 11; Supplemental Figures 14A–14C) (Marcussen et al., 2014; Xiang et al., 2019; Zhao et al., 2024). Transcriptomic data from 2018 failed to identify grain-specific *TaFie* expression, possibly due to the absence of early grain samples in that dataset (Ramirez-Gonzalez et al., 2018).

Although the orthology relationships of prolamins are difficult to determine, their regulatory sequences and upstream transcriptional activators are relatively conserved. For example, O2 regulates zein expression in maize, whereas OsbZIP58/RISBZ1 regulates prolamins in rice. The epigenetic regulatory modules identified in this study are present in rice, maize, and wheat (Chen et al., 2024), indicating that they are universally conserved in grasses. However, the specific correlations and regulatory scope differ among species. In rice, the *osfie1* mutant does not show increased levels of 13-kDa prolamins in mature grain (Supplemental Figure 13), and *osfie2* mutants do not exhibit elevated prolamin content (Cheng et al., 2020). In wheat, a weak mutant affecting three ubiquitously expressed TaFie members shows elevated gliadin and low-molecular-weight glutenin content (Chen et al., 2024).

Taken together, our findings reveal a conserved function of ZmFie1/OsFie1-mediated H3K27me3 deposition in cereal endosperm development. The newly evolved, grain-specific FIE1-PRC2 complex in cereals plays a key role in balancing storage substance synthesis and cell proliferation during persistent endosperm development.

Epigenetic modifications play crucial roles in plant growth, development, and environmental adaptation, yet their specific

functions in cereal endosperm development remain poorly understood. The application of CUT&Tag technology has greatly facilitated the identification of downstream targets of various epigenetic marks. Future research should aim to further elucidate and harness these modifications for crop improvement. The utilization of epigenetic regulation holds significant potential for advancing genetic breeding programs in cereal crops.

METHODS

Genetic materials

Maize plants were grown in the Songjiang field in Shanghai, China, for the summer nursery, and in the Damao field in Sanya, China, for the winter nursery. To create *ZmFie1* knockout alleles using CRISPR-Cas9, guide RNA target sites for *ZmFie1* were selected using the E-CRISP website (http://www.e-crisp.org/E-CRISP/designcrispr.html), and the sequence ACTTCCACCCTACCGAGGT was chosen as the guide RNA. The CRISPR-Cas9 constructs were transformed into the KN5585 inbred line by Wimi Biotechnology (Jiangsu). Several independent T_0 plants were backcrossed to WT KN5585 to produce BC_1 seeds. The BC_1 seeds were planted, and heterozygous *zmfie1* seedlings were screened to obtain construct-free *zmfie1-1* and *zmfie1-2* lines. Homozygous *zmfie1-1* and *zmfie1-2* mutants from the BC_1F_2 generation were used for subsequent experiments.

Specifically, the *zmfie1-2* allele contains a 29-bp insertion. We designed a pair of primers (W1056 + W1058; Supplemental Data 12) flanking this insertion for PCR amplification. The WT band is 224 bp, and the *zmfie1-2* band is 253 bp, which can be distinguished in a 3% agarose gel (Supplemental Figure 6D).

The EMS-induced allele *zmfie1-3*, in the B73 background, was obtained from the Maize EMS-induced Mutant Database (MEMD) (http://www.elabcaas.cn/memd/, mutant ID: EMS4-11248d) (Lu et al., 2018). Heterozygous *zmfie1-3* plants were subjected to linkage analysis using a method similar to that used for *zmfie1-2*, and genotyping was performed using a KASP (Kompetitive Allele-Specific PCR; LGC) marker.

Oryza sativa L. cultivar Kitaake and *osfie1* were obtained from Yangzhou University, China (Cheng et al., 2020). The plants were grown in plastic pots filled with paddy-field soil in a greenhouse under a 13-h light (28°C)/11-h dark (26°C) photoperiod. The point-awn method was used to mark rice grains that flowered on the same day and caryopses were collected at 5–7 DAP for H3K27me3 CUT&Tag and semi-thin sectioning.

CUT&Tag

The maize inbred line B73 used for CUT&Tag was grown and self-pollinated in the Tai'an experimental field in Shandong, China. Fresh endosperm samples were collected during early to filling stages (4, 6, 8, 10, and 12 DAP) and samples from two ears were pooled. Approximately 200–500 mg of endosperm tissue was transferred to 1× washing buffer (TD904, Vazyme, China), crushed using a grinding rod, filtered through a 40-μm filter (BD Biosciences, 352340), and transferred to a fresh tube. Next, 5 μl of the nuclear suspension was mixed with 1/40 DAPI solution (10 μg/ml stock, Solarbio). The concentration of nuclei and presence of impurities were assessed under a microscope. A total of 100 000 nuclei were used for each CUT&Tag experiment. The procedure followed the manufacturer's protocol (TD904, Vazyme, China); the incubation time for the nuclei suspension and magnetic beads was extended to 20 min. For the 20-DAP endosperm samples, nuclei were sorted by flow cytometry prior to CUT&Tag. Flow cytometry protocols were described previously (Ji et al., 2022); these utilized a Moflo XDP flow cytometer (Beckman Coulter). CUT&Tag reactions were incubated overnight at 4°C with 1 μg of anti-H3K27me3 antibody (ABclonal, A22006). Libraries were amplified for 10–12 cycles and sequenced on an Illumina NovaSeq platform by JMDNA (Shanghai) Bio-Medical Technology.

ChIP-seq and RNA-seq

In the spring of 2023, seeds of heterozygous WT/*zmfie1-1* plants were sown in the Songjiang experimental field in Shanghai, China. Three ears were harvested at 10 DAP. The endosperm was extracted, rapidly frozen in liquid nitrogen, and stored at −80°C. Approximately 2 g of endosperm tissue was ground in liquid nitrogen, dissolved in M1 buffer, and cross-linked with 1% formaldehyde for 10 min. ChIP experiments were performed according to a published protocol (Kaufmann et al., 2010), using 10 μg of anti-H3K27me3 antibody (ABclonal, A22007). A modified ChIP elution buffer was used, consisting of 1% (w/v) SDS and 0.1 M $NaHCO_3$. DNA was purified using the QIAquick PCR Purification Kit (Qiagen). ChIP-DNA libraries were constructed with 1–5 ng of DNA using the VAHTS Universal DNA Library Prep Kit for MGI (NDM607, Vazyme, China) and sequenced on an MGI T7 platform by JMDNA (Shanghai) Bio-Medical Technology.

Bioinformatics data preprocessing and alignment

Seventeen gigabases of raw reads were processed using fastp (version 0.20.1) with the "–detect_adapter_for_pe" parameter to filter reads, trim low-quality bases, and remove adapters. Subsequently, FastQC (version 0.11.9) was used for quality assessment of the clean data (https://github.com/s-andrews/FastQC).

All DNA sequencing data, including CUT&Tag, ChIP-seq, and RNA-seq, were aligned to the maize B73_v4 reference genome, accessible at: https://ftp.ensemblgenomes.ebi.ac.uk/pub/plants/release-45/fasta/zea_mays/dna/. Clean reads from CUT&Tag, ChIP-seq, and RNA-seq were mapped to the B73_v4 genome using Bowtie2 (version 2.2.4) with the parameters "-I 0 -X 500 –no-discordant.'' Alignment rates were used to evaluate sample quality. Duplicate reads were removed using the MarkDuplicates module in GATK software with the parameter "-REMOVE_DUPLICATES true"; only reads with MAPQ 5 were retained for downstream analysis.

Peak calling for histone CUT&Tag data was performed using MACS2, with the parameters "-g 2.1e9 -f BAMPE -B -q 1e−5 –broad –broad-cutoff 0.1 –keep-dup all.'' The ChIPseeker package with default parameters was used to annotate peaks. Genes located within 2 kb of a peak were considered potential targets. Differential peak enrichment was identified using the DiffBind R package with the DESeq2 method, applying thresholds of FDR < 0.05 and FC ≥ 1.5.

The BAM files were converted to BigWig format and normalized to reads per kilobase per million mapped reads, with a 10-bp bin size, using the bamCoverage command in deepTools.

Clustering analysis was performed with Short Time-series Expression Miner (STEM) software (Ernst and Bar-Joseph, 2006) using the expression data of the FSP gene set from En6 to En38. STEM analysis was conducted using the online platform available at https://cloud.oebiotech.com/task/. Six significant profiles were identified out of 50 profiles, and trend graphs and clustering heatmaps of these significant modules were generated.

Phenotypic and histocytochemical analysis

Kernels selected from the middle region of ears with uniform kernel set were used for photography and kernel trait measurements. More than 100 kernels were measured per ear. Kernel length, width, and weight were assessed using the automatic seeds test system (SC-G, Hangzhou Wanshen Detection Technology).

To minimize developmental variation caused by temperature, plants of different genotypes were pollinated on the same day, and samples were

collected accordingly. Samples were fixed in FAA solution, embedded in resin, and collected from five ears per genotype at each developmental stage. Fixation, embedding, photography, and statistical analysis were performed according to a published protocol (Ji et al., 2022). In Figure 5A, scanned cross-sectional images of kernels were obtained using high-resolution nano-computed tomography (CT). Kernels were fixed in FAA solution, subjected to gradient dehydration and soaked in 2% iodine solution for 48 h. After triple washing with absolute ethanol, samples were vacuum-dried and scanned using a high-resolution nano-CT device (SkyScan 2214, Bruker, Kontich, Belgium).

Cytological linkage analysis was performed as follows: ears from heterozygous *zmfie1-3* plants were self-pollinated and harvested at 16 DAP. Kernels with regular shapes from the middle of each ear were selected and fixed in FAA solution. A small portion of the endosperm was used for individual genotyping. Kernels of the same genotype were pooled, embedded in resin, and semi-thin sectioned. Sections were photographed and statistically analyzed according to a published protocol (Ji et al., 2022). Samples were stained with 0.1% toluidine blue solution and imaged under bright field using a ZEISS Axio Zoom.V16 microscope for overview imaging, or a Leica DM2500 for higher magnification.

Determination of starch and protein contents

Five ears were collected for each genotype, and two kernels from each ear were ground together to produce flour for subsequent measurements. Each genotype had five biological replicates. Starch content was measured using the Megazyme Total Starch Assay Kit (catalog number K-TSTA-50A) according to the manufacturer's protocol (Zhang et al., 2015). Zein and non-zein proteins were extracted following a laboratory-established protocol (Zheng et al., 2019). Zein accumulation patterns were analyzed by electrophoresis using 15% SDS–PAGE gels. Total nitrogen content was determined using a Dumas rapid nitrogen analyzer (Elementar), according to an existing laboratory protocol (Huang et al., 2022).

Protein extraction from rice seeds was performed according to a published protocol (Kawakatsu et al., 2010).

RT-qPCR analysis

Total RNA was extracted from immature rice seeds using TRIzol. One microgram of total RNA was used for first-strand cDNA synthesis with the HiScript II Q RT SuperMix for qPCR (Vazyme, R223). Primers for RT-qPCR in rice were obtained from the referenced study (Kawakatsu et al., 2010). The primer sequences and corresponding gene information are listed in Supplemental Data 12.

Accession numbers

The CUT&Tag, ChIP-seq, and RNA-seq datasets have been deposited in the National Center for Biotechnology Information database under accession code BioProject PRJNA1172298 (https://www.ncbi.nlm.nih.gov/).

ACKNOWLEDGMENTS

We extend our gratitude to Professor Chen Chen from Yangzhou University for providing the *osfie1* mutant. We thank Professor Jinchen Long from the CAS Center for Excellence in Molecular Plant Sciences for assistance with Cut&Tag and ChIP-seq analyses. Our appreciation goes to Professor Yin Li from Huazhong University of Science and Technology for wheat transcriptomic data analysis. We are also grateful to Mr. Xiaoyan Gao and Miss Jiqin Li (CEMPS) for their histocytochemical analysis support. Special thanks are due to Dr. Xiaowei Zhang (CEMPS) for facilitating the use of the ZEISS Axio Zoom.V16 microscope, as well as to Dr. Yanxia Mai (CEMPS) for her assistance with flow cytometry. This work was supported by the National Natural Science Foundation of China (U22A20466 to G.W., 32272146 and 31871626 to J.W., 32525007 to Y.W.), the Natural Science Foundation of Shanghai (23ZR1470400 to J.W. and 22ZR1469400 to Y.W.), the XPLORER PRIZE, NEW CORNERSTONE SCIENCE FOUNDATION (to Y.W.), the Shanghai Academy of Natural Sciences (SANS, to Y.W.), and the Strategic Priority Research Program of the Chinese Academy of Sciences (XDB1120100 to Y.W.). No conflict of interest is declared.

AUTHOR CONTRIBUTIONS

J.W., S.L., L.W., D.S., L.X., Z.Z., Y.Wang, C.J., Y.C., X.Z., F.Z., M.L, X.Li, C.D., and Q.W. conducted the experiments. Y.Wu. supervised the project. J.W., S.L., X.Lu., W.W., G.W., and Y.Wu. interpreted the data. J.W. and Y. Wu. drafted and edited the manuscript.

SUPPLEMENTAL INFORMATION

Supplemental information is available at *Plant Communications Online*.

Received: November 11, 2024
Revised: March 6, 2025
Accepted: April 17, 2025
Published: April 22, 2025

REFERENCES

Anderson, S.N., Zhou, P., Higgins, K., Brandvain, Y., and Springer, N. M. (2021). Widespread imprinting of transposable elements and variable genes in the maize endosperm. PLoS Genet. **17**:e1009491. https://doi.org/10.1371/journal.pgen.1009491.

Chen, B., Maas, L., Figueiredo, D., Zhong, Y., Reis, R., Li, M., Horstman, A., Riksen, T., Weemen, M., Liu, H., et al. (2022). BABY BOOM regulates early embryo and endosperm development. Proc. Natl. Acad. Sci. USA **119**:e2201761119. https://doi.org/10.1073/pnas.2201761119.

Chen, J., Zeng, B., Zhang, M., Xie, S., Wang, G., Hauck, A., and Lai, J. (2014). Dynamic transcriptome landscape of maize embryo and endosperm development. Plant Physiol. **166**:252–264. https://doi.org/10.1104/pp.114.240689.

Chen, J., Zhao, L., Li, H., Yang, C., Lin, X., Lin, Y., Zhang, H., Zhang, M., Bie, X., Zhao, P., et al. (2024). NUCLEAR FACTOR-Y-POLYCOMB REPRESSIVE COMPLEX2 dynamically orchestrates starch and seed storage protein biosynthesis in wheat. Plant Cell **36**:4786–4803. https://doi.org/10.1093/plcell/koae256.

Cheng, X., Pan, M., E, Z., Zhou, Y., Niu, B., and Chen, C. (2020). Functional divergence of two duplicated Fertilization Independent Endosperm genes in rice with respect to seed development. Plant J. **104**:124–137. https://doi.org/10.1111/tpj.14911.

Danilevskaya, O.N., Hermon, P., Hantke, S., Muszynski, M.G., Kollipara, K., and Ananiev, E.V. (2003). Duplicated fie genes in maize: expression pattern and imprinting suggest distinct functions. Plant Cell **15**:425–438. https://doi.org/10.1105/tpc.006759.

Dong, J., Feng, Y., Kumar, D., Zhang, W., Zhu, T., Luo, M.C., and Messing, J. (2016). Analysis of tandem gene copies in maize chromosomal regions reconstructed from long sequence reads. Proc. Natl. Acad. Sci. USA **113**:7949–7956. https://doi.org/10.1073/pnas.1608775113.

Ernst, J., and Bar-Joseph, Z. (2006). STEM: a tool for the analysis of short time series gene expression data. BMC Bioinf. **7**:191. https://doi.org/10.1186/1471-2105-7-191.

Fu, Y., Li, S., Xu, L., Ji, C., Xiao, Q., Shi, D., Wang, G., Wang, W., Wang, J., Wang, J., et al. (2023). RNA sequencing of cleanly isolated early endosperms reveals coenocyte-to-cellularization transition features in maize. Seed Biology **2**:1–10. https://doi.org/10.48130/SeedBio-2023-0008.

Grossniklaus, U., Vielle-Calzada, J.P., Hoeppner, M.A., and Gagliano, W.B. (1998). Maternal control of embryogenesis by MEDEA, a polycomb group gene in Arabidopsis. Science **280**:446–450. https://doi.org/10.1126/science.280.5362.446.

Gutierrez-Marcos, J.F., Costa, L.M., Dal Pra, M., Scholten, S., Kranz, E., Perez, P., and Dickinson, H.G. (2006). Epigenetic asymmetry of imprinted genes in plant gametes. Nat. Genet. **38**:876–878. https://doi.org/10.1038/ng1828.

He, W., Wang, L., Lin, Q., and Yu, F. (2021). Rice seed storage proteins: Biosynthetic pathways and the effects of environmental factors. J. Integr. Plant Biol. **63**:1999–2019. https://doi.org/10.1111/jipb.13176.

Huang, X., Lu, Z., Wang, X., Ouyang, Y., Chen, W., Xie, K., Wang, D., Luo, M., Luo, J., and Yao, J. (2016). Imprinted gene OsFIE1 modulates rice seed development by influencing nutrient metabolism and modifying genome H3K27me3. Plant J. **87**:305–317. https://doi.org/10.1111/tpj.13202.

Huang, Y., Wang, H., Zhu, Y., Huang, X., Li, S., Wu, X., Zhao, Y., Bao, Z., Qin, L., Jin, Y., et al. (2022). THP9 enhances seed protein content and nitrogen-use efficiency in maize. Nature **612**:292–300. https://doi.org/10.1038/s41586-022-05441-2.

Itoh, H., Shimada, A., Ueguchi-Tanaka, M., Kamiya, N., Hasegawa, Y., Ashikari, M., and Matsuoka, M. (2005). Overexpression of a GRAS protein lacking the DELLA domain confers altered gibberellin responses in rice. Plant J. **44**:669–679. https://doi.org/10.1111/j.1365-313X.2005.02562.x.

Ji, C., Xu, L., Li, Y., Fu, Y., Li, S., Wang, Q., Zeng, X., Zhang, Z., Zhang, Z., Wang, W., et al. (2022). The O2-ZmGRAS11 transcriptional regulatory network orchestrates the coordination of endosperm cell expansion and grain filling in maize. Mol. Plant **15**:468–487. https://doi.org/10.1016/j.molp.2021.11.013.

Kang, I.H., Steffen, J.G., Portereiko, M.F., Lloyd, A., and Drews, G.N. (2008). The AGL62 MADS domain protein regulates cellularization during endosperm development in Arabidopsis. Plant Cell **20**:635–647. https://doi.org/10.1105/tpc.107.055137.

Kaufmann, K., Muiño, J.M., Østerås, M., Farinelli, L., Krajewski, P., and Angenent, G.C. (2010). Chromatin immunoprecipitation (ChIP) of plant transcription factors followed by sequencing (ChIP-SEQ) or hybridization to whole genome arrays (ChIP-CHIP). Nat. Protoc. **5**:457–472. https://doi.org/10.1038/nprot.2009.244.

Kawakatsu, T., Hirose, S., Yasuda, H., and Takaiwa, F. (2010). Reducing rice seed storage protein accumulation leads to changes in nutrient quality and storage organelle formation. Plant Physiol. **154**:1842–1854. https://doi.org/10.1104/pp.110.164343.

Kohler, C., Hennig, L., Bouveret, R., Gheyselinck, J., Grossniklaus, U., and Gruissem, W. (2003). Arabidopsis MSI1 is a component of the MEA/FIE Polycomb group complex and required for seed development. EMBO J. **22**:4804–4814. https://doi.org/10.1093/emboj/cdg444.

Leroux, B.M., Goodyke, A.J., Schumacher, K.I., Abbott, C.P., Clore, A. M., Yadegari, R., Larkins, B.A., and Dannenhoffer, J.M. (2014). Maize early endosperm growth and development: from fertilization through cell type differentiation. Am. J. Bot. **101**:1259–1274. https://doi.org/10.3732/ajb.1400083.

Lu, X., Liu, J., Ren, W., Yang, Q., Chai, Z., Chen, R., Wang, L., Zhao, J., Lang, Z., Wang, H., et al. (2018). Gene-Indexed Mutations in Maize. Mol. Plant **11**:496–504. https://doi.org/10.1016/j.molp.2017.11.013.

Macrae, T.A., Fothergill-Robinson, J., and Ramalho-Santos, M. (2023). Regulation, functions and transmission of bivalent chromatin during mammalian development. Nat. Rev. Mol. Cell Biol. **24**:6–26. https://doi.org/10.1038/s41580-022-00518-2.

Marcussen, T., Sandve, S.R., Heier, L., Spannagl, M., Pfeifer, M., International Wheat Genome Sequencing Consortium, Jakobsen, K.S., Wulff, B.B.H., Steuernagel, B., Mayer, K.F.X., and Olsen, O. A. (2014). Ancient hybridizations among the ancestral genomes of bread wheat. Science **345**:1250092. https://doi.org/10.1126/science.1250092.

Masiero, S., Colombo, L., Grini, P.E., Schnittger, A., and Kater, M.M. (2011). The emerging importance of type I MADS box transcription factors for plant reproduction. Plant Cell **23**:865–872. https://doi.org/10.1105/tpc.110.081737.

Ni, J., Ma, X., Feng, Y., Tian, Q., Wang, Y., Xu, N., Tang, J., and Wang, G. (2019). Updating and interaction of polycomb repressive complex 2 components in maize (Zea mays). Planta **250**:573–588. https://doi.org/10.1007/s00425-019-03193-4.

Ohad, N., Yadegari, R., Margossian, L., Hannon, M., Michaeli, D., Harada, J.J., Goldberg, R.B., and Fischer, R.L. (1999). Mutations in FIE, a WD polycomb group gene, allow endosperm development without fertilization. Plant Cell **11**:407–416. https://doi.org/10.1105/tpc.11.3.407.

Olsen, O.A. (2001). ENDOSPERM DEVELOPMENT: Cellularization and Cell Fate Specification. Annu. Rev. Plant Physiol. Plant Mol. Biol. **52**:233–267. https://doi.org/10.1146/annurev.arplant.52.1.233.

Portereiko, M.F., Lloyd, A., Steffen, J.G., Punwani, J.A., Otsuga, D., and Drews, G.N. (2006). AGL80 is required for central cell and endosperm development in Arabidopsis. Plant Cell **18**:1862–1872. https://doi.org/10.1105/tpc.106.040824.

Ramirez-Gonzalez, R.H., Borrill, P., Lang, D., Harrington, S.A., Brinton, J., Venturini, L., Davey, M., Jacobs, J., van Ex, F., Pasha, A., et al. (2018). The transcriptional landscape of polyploid wheat. Science **361**:eaar6089. https://doi.org/10.1126/science.aar6089.

Song, X.J., Huang, W., Shi, M., Zhu, M.Z., and Lin, H.X. (2007). A QTL for rice grain width and weight encodes a previously unknown RING-type E3 ubiquitin ligase. Nat. Genet. **39**:623–630. https://doi.org/10.1038/ng2014.

Sorensen, M.B., Chaudhury, A.M., Robert, H., Bancharel, E., and Berger, F. (2001). Polycomb group genes control pattern formation in plant seed. Curr. Biol. **11**:277–281. https://doi.org/10.1016/s0960-9822(01)00072-0.

Springer, N.M., Danilevskaya, O.N., Hermon, P., Helentjaris, T.G., Phillips, R.L., Kaeppler, H.F., and Kaeppler, S.M. (2002). Sequence relationships, conserved domains, and expression patterns for maize homologs of the polycomb group genes E(z), esc, and E(Pc). Plant Physiol. **128**:1332–1345. https://doi.org/10.1104/pp.010742.

Sreenivasulu, N., and Wobus, U. (2013). Seed-development programs: a systems biology-based comparison between dicots and monocots. Annu. Rev. Plant Biol. **64**:189–217. https://doi.org/10.1146/annurev-arplant-050312-120215.

Strejckova, B., Cegan, R., Pecinka, A., Milec, Z., and Safar, J. (2020). Identification of polycomb repressive complex 1 and 2 core components in hexaploid bread wheat. BMC Plant Biol. **20**:175. https://doi.org/10.1186/s12870-020-02384-6.

Tonosaki, K., Ono, A., Kunisada, M., Nishino, M., Nagata, H., Sakamoto, S., Kijima, S.T., Furuumi, H., Nonomura, K.I., Sato, Y., et al. (2021). Mutation of the imprinted gene OsEMF2a induces autonomous endosperm development and delayed cellularization in rice. Plant Cell **33**:85–103. https://doi.org/10.1093/plcell/koaa006.

Wang, D., Li, F., Cao, S., and Zhang, K. (2020a). Genomic and functional genomics analyses of gluten proteins and prospect for simultaneous improvement of end-use and health-related traits in wheat. Theor. Appl. Genet. **133**:1521–1539. https://doi.org/10.1007/s00122-020-03557-5.

Wang, Y., Jiang, H., and Wang, G. (2020b). PHERES1 Controls Endosperm Gene Imprinting and Seed Development. Trends Plant Sci. **25**:517–519.

Wu, X., Xie, L., Sun, X., Wang, N., Finnegan, E.J., Helliwell, C., Yao, J., Zhang, H., Wu, X., Hands, P., et al. (2023). Mutation in Polycomb repressive complex 2 gene OsFIE2 promotes asexual embryo

formation in rice. Nat. Plants **9**:1848–1861. https://doi.org/10.1038/s41477-023-01536-4.

Xiang, D., Quilichini, T.D., Liu, Z., Gao, P., Pan, Y., Li, Q., Nilsen, K.T., Venglat, P., Esteban, E., Pasha, A., et al. (2019). The Transcriptional Landscape of Polyploid Wheats and Their Diploid Ancestors during Embryogenesis and Grain Development. Plant Cell **31**:2888–2911. https://doi.org/10.1105/tpc.19.00397.

Xu, J.-H., and Messing, J. (2008). Diverged copies of the seed regulatory Opaque-2 gene by a segmental duplication in the progenitor genome of rice, sorghum, and maize. Mol. Plant **1**:760–769.

Xurun, Y., Xinyu, C., Liang, Z., Jing, Z., Heng, Y., Shanshan, S., Fei, X., and Zhong, W. (2015). Structural development of wheat nutrient transfer tissues and their relationships with filial tissues development. Protoplasma **252**:605–617. https://doi.org/10.1007/s00709-014-0706-0.

Yang, T., Wu, X., Wang, W., and Wu, Y. (2023). Regulation of seed storage protein synthesis in monocot and dicot plants: A comparative review. Mol. Plant **16**:145–167. https://doi.org/10.1016/j.molp.2022.12.004.

Yuan, Y., Huo, Q., Zhang, Z., Wang, Q., Wang, J., Chang, S., Cai, P., Song, K.M., Galbraith, D.W., Zhang, W., et al. (2024). Decoding the gene regulatory network of endosperm differentiation in maize. Nat. Commun. **15**:34. https://doi.org/10.1038/s41467-023-44369-7.

Zhang, J., Zhang, Z., Zhang, R., Yang, C., Zhang, X., Chang, S., Chen, Q., Rossi, V., Zhao, L., Xiao, J., et al. (2024a). Type I MADS-box transcription factor TaMADS-GS regulates grain size by stabilizing cytokinin signalling during endosperm cellularization in wheat. Plant Biotechnol. J. **22**:200–215. https://doi.org/10.1111/pbi.14180.

Zhang, S., Mohanty, D., Muzaffar, A., and Ni, M. (2024b). Two MADS-box proteins, AGL9 and AGL15, recruit the FIS-PRC2 complex to trigger the phase transition from endosperm proliferation to embryo development in Arabidopsis. Mol. Plant **17**:1110–1128. https://doi.org/10.1016/j.molp.2024.05.011.

Zhang, Z., Yang, J., and Wu, Y. (2015). Transcriptional regulation of zein gene expression in maize through the additive and synergistic action of opaque2, prolamine-box binding factor, and O2 heterodimerizing proteins. Plant Cell **27**:1162–1172.

Zhao, D., Chen, Z., Xu, L., Zhang, L., and Zou, Q. (2021). Genome-Wide Analysis of the MADS-Box Gene Family in Maize: Gene Structure, Evolution, and Relationships. Genes **12**:1956. https://doi.org/10.3390/genes12121956.

Zhao, L., Chen, J., Zhang, Z., Wu, W., Lin, X., Gao, M., Yang, Y., Zhao, P., Xu, S., Yang, C., et al. (2024). Deciphering the Transcriptional Regulatory Network Governing Starch and Storage Protein Biosynthesis in Wheat for Breeding Improvement. Adv. Sci. **11**:e2401383. https://doi.org/10.1002/advs.202401383.

Zheng, X., Li, Q., Li, C., An, D., Xiao, Q., Wang, W., and Wu, Y. (2019). Intra-Kernel Reallocation of Proteins in Maize Depends on VP1-Mediated Scutellum Development and Nutrient Assimilation. Plant Cell **31**:2613–2635. https://doi.org/10.1105/tpc.19.00444.

Zhu, D., Wen, Y., Yao, W., Zheng, H., Zhou, S., Zhang, Q., Qu, L.J., Chen, X., and Wu, Z. (2023). Distinct chromatin signatures in the Arabidopsis male gametophyte. Nat. Genet. **55**:706–720. https://doi.org/10.1038/s41588-023-01329-7.

Larkins, B.A., Wu, Y., Song, R., and Messing, J. (2017). Maize seed storage proteins. In Maize Kernel Development, B.A. Larkins, ed. (Oxfordshire: CABI), **14**:pp. 175–189.